C 1 Amphiphilic Systems

H. Frielinghaus
Jülich Centre for Neutron Science,
Institut für Festkörperforschung
Forschungszentrum Jülich GmbH

Contents

1 Introduction

In today's life the best known examples for amphiphilic molecules are soap and detergents. These agents lower the surface tension of water, which allows for wetting almost any surface. Furthermore, oily substances can be taken up in solution. In both cases, the surfactant is active at the surface. The hydrophilic head group points towards the water while the hydrophobic tail points towards the dissolved oil droplet or the non-polar surface. In this sense, the surfactant is an amphiphile, which mediates between polar solvents and non-polar solutes or surfaces. This property is highly interesting for many nowadays industrial products. For food, cosmetic and pharmaceutic products oily substances are to be taken up in aqueous solution. One might think of salad dressings or low fat margarines, lotions and creams. Pharmaceutical agents are often non-polar and need to be in aqueous solution for the ingestion. Most of these industrial products are emulsions. By mechanical mixing and amphiphilic stabilization the non-polar substances are kept in aqueous solution for long times. This finite stability leads to finite best-before-dates, but the amphiphile concentration can be kept low. In fundamental research one often prefers microemulsions with higher surfactant concentrations and thermodynamic (i.e. infinite) stability. Then, the system is always well defined and does not depend on the history of preparation.
The property of amphiphiles to orient themselves towards the non-polar and polar regions is called self-assembly. This effect holds for surfactants, which usually appear with molar masses of several hundred Daltons. But also long chain molecules can be amphiphilic. The easiest case is a symmetric linear chain with one end being hydrophilic and the other hydrophobic, a symmetric amphiphilic block copolymer. Such polymers proved to be efficiency boosters in microemulsions. This molecule allows for dissolving oil in water with much less surfactant. The polymer ends are dissolved in the oil and water domains and form coils on either side of the membrane. The coils exert some force on the surfactant membrane, which leads to flattening. This allows for the formation of larger oil and water domains with a better surface to volume ratio and so surfactant can be saved. This polymer example shows that self-assembly is not limited to small molecules. The effective interaction of the polymer is larger due to its length, and so the difference between hydrophobic and hydrophilic can be relaxed for the self-assembly effect. So small miscibility differences of polymers might still result in ordered structures. Most structures of amphiphiles (surfactants and polymers) are of the nanometer scale. This length scale is accessed by electron microscopy and by (neutron and x-ray) scattering experiments. The structural information in combination with theories leads to the fundamental understanding of the mechanisms. Only with this knowledge, modern products can be developed because the systems are getting more and more complex with more and more substances. Amphiphilic polymers are the key substance for emulsification problems in the future.

2 Aqueous Surfactant Solutions

Surfactants can be divided into two major classes: Ionic surfactants possess a ionic head group with a counterion while non-ionic surfactants have no charges. In the first case, the ionic head group is soluble in water, and the counterion dissociates. One for research important surfactant is the sodium dodecyl sulfate (SDS, see Fig. 1). The SDS is an anionic surfactant because the sulfate head group is an anion. The tail of the SDS molecule is a hydrocarbon, which is typical for most of the surfactants. A representative for the non-ionic surfactants is tetraethyleneglycol-

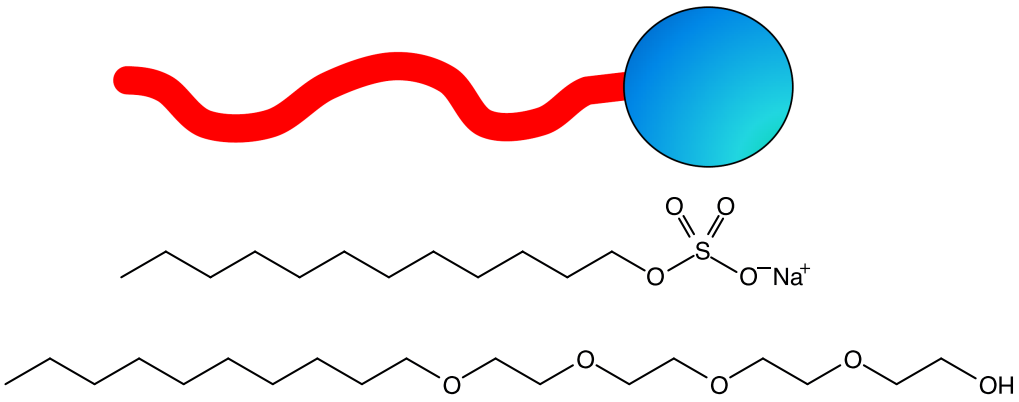

Fig. 1: *Top: Conceptual drawing of a surfactant molecule. The hydrophilic head is blue while the hydrophobic tail is red. Middle: Chemical structure of sodium dodecyl sulfate (SDS). The head and tail groups are just below the conceptual drawing. Bottom: Chemical structure of tetraethyleneglycolmonodecylether ($C_{10}E_4$). The head group is four glycol groups long.*

monodecylether ($C_{10}E_4$, the indices count the carbon atoms and ethylene oxide groups, see Fig. 1). The head group is not charged; but the oxygen atoms along the head group give rise to hydrogen bonding, which is favorable for the water solubility. For this type of surfactant the molecule ends can vary in length, but also in chemical structure. For instance the hydrophobic tails can possess different amounts of saturated carbon-carbon bonds. This is important for lipids, which are natural ionic surfactants forming cell membranes. Lipids often have two hydrophobic tails. The number of double-bonds in the tails determines the thermodynamic state of the membrane. Many unsaturated tails give rise to crystalline order of the hydrophobic tails [11]. Apart from the tails, the head groups may possess two oppositely charged groups; then the surfactant is called amphoteric. The whole concept of hydrophilic and hydrophobic can be extended by a third type of philicity: The polymer Teflon (fluorinated carbon chains) is known to be neither water soluble nor oil soluble. If fluorinated carbon chains are used as hydrophobic tails a new class of surfactants is obtained[1]. Throughout this manuscript we limit ourselves to the simple twofold concept of hydrophilicity and lipophilicity. The interested reader may find further information about fluorinated surfactants in the literature [1].

We now consider aqueous solutions of a single surfactant type. It is known that at very low concentrations the surfactant molecules are dissolved independently. The reason for this behavior is the entropy, which favors dissociated molecules. But because the hydrophobic tail causes some enthalpic violation, at the critical micelle concentration (CMC) the surfactant molecules associate and form small spherical micelles. The hydrophobic tails are in the center and the hydrophilic heads surround the micelle. The hydrophobic neighborhood of the hydrocarbon chains can be monitored by NMR [2] and so very precise values for the CMC can be given. The effect of the CMC is a volume effect and is thus determined for large volumes. At the surface, the surfactant molecules can also be found. These studies focus on Langmuir-Blodgett films for instance, but this topic will lead too far.

The next question focuses on the state or structure of the micelles in solution. Different structures can be classified and shall be explained on the basis of a simple model, which mainly focuses on ionic surfactants. The parameter of interest is the packing parameter [3], which is

[1] Fluorinated surfactants allow for CO_2 to be used as hydrophobic component in microemulsions for instance.

Table 1: *The different micellar structures predicted on the basis of the packing parameter.*

P	molecule geometry	micelle structure	symmetry
$< \frac{1}{3}$	cone	sphere	point-like
$\frac{1}{3}$ to $\frac{1}{2}$	wedge	cylinder	cylinder
$\frac{1}{2}$ to 1	wedge	vesicle (double layer)	point-like
1	cylinder	planar double layer	plane-like

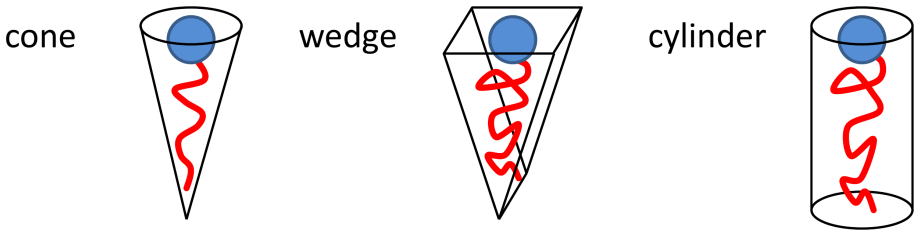

Fig. 2: *Molecule geometries for different packing parameters.*

defined as follows:

$$P = \frac{v}{a \cdot l} \tag{1}$$

In this equation the parameter v is the volume of the whole molecule, a is the area of the head group, and l is the length of the chain. This packing parameter can vary between values below $\frac{1}{3}$ and 1 (see Table 1). For values below $\frac{1}{3}$ the micelles are spherical, then for P up to $\frac{1}{2}$ the micelles are elongated cylinders. For P up to 1 the micelles form closed double layers, i.e. spherical hollow membranes; they are called vesicles. For $P = 1$ the membranes become planar. It shall be mentioned that this effect is called self-assembly already. The formed structures have a high degree of symmetry. Only fluctuations might destroy the high degree of symmetry. So for instance very long cylindrical micelles start to bend and a worm-like micelle is formed [4]. For the purpose of this lecture we restrict the considerations of P to a maximum of 1.
An experimental phase diagram is depicted in Fig. 3. We first restrict ourselves to the temperature of 20°C (see Fig. 3). The CMC is found at concentrations of around 0.005%. At higher concentrations up to ca. 1% spherical micelles are found. In between 1 and 10% the micelles become cylindrical. Going up in temperature now, their length grows until the phase boundary at ∼33°C is reached. A clear line between spherical and cylindrical micelles is not given in the phase diagram because the phase transition smears out, and usually a coexistence between the two morphologies is found. The long micelles are usually wormlike because of the fluctuations. At higher concentrations the worms can even form networks. All these effects take place in the one-phase region (1Φ or L_1). The temperature has an effect on the micelle shape because at lower temperatures water penetrates the head group of the non-ionic surfactant.
So far we did not consider the case, that the micelles can be reversed. At low water concentrations (or high surfactant concentrations) the water and hydrophilic heads form a closed volume surrounded by the hydrophobic parts. The corresponding region is indicated by L_2 or 1Φ. The interesting case of the L_3-phase is found at slightly higher temperatures. Then the membranes fill the whole volume with a sponge like structure. The membranes are strongly fluctuating. The more planar membranes are found in the L_α-phase at relatively high concentrations. These

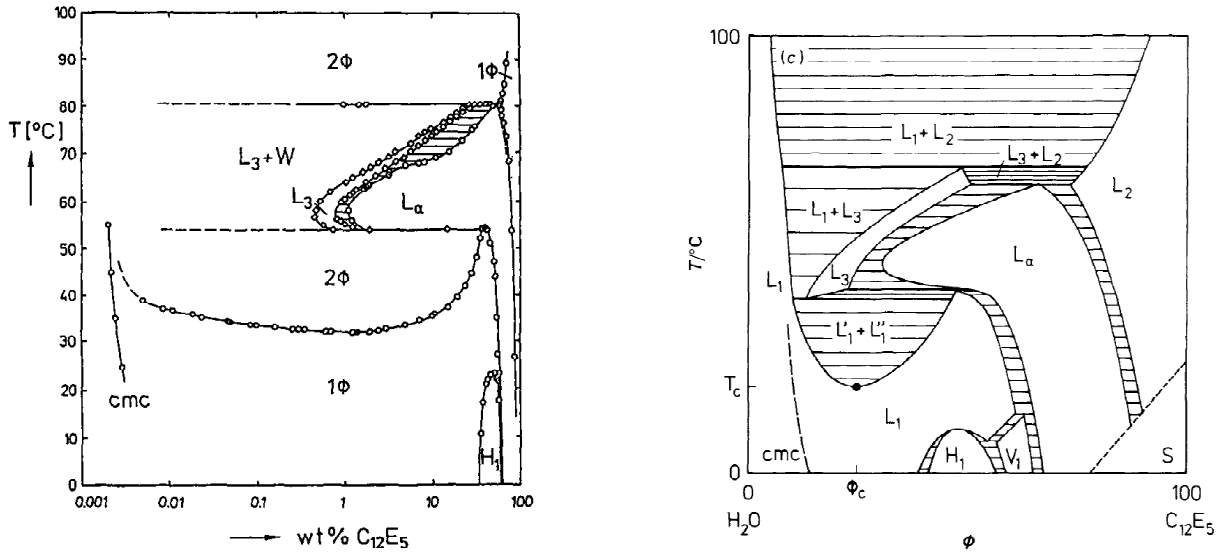

Fig. 3: *An experimental phase diagram of the non-ionic surfactant $C_{12}E_5$ in water [5, 6]. Following a horizontal line at ca. 20°C from low to higher concentrations one finds the CMC at around 0.005% and the one-phase (1Φ) region. Below ∼1% the micelles are spherical and uncorrelated. Between 1 and 10% the micelles become cylindrical. Their length increases with temperature until the phase boundary at around 33°C is reached. Interestingly, more phases are found than predicted by the simple packing parameter approach. 2-phase coexistence is indicated by 2Φ. The hexagonal phase is indicated by H_1 and the lamellar phase by L_α. The L_3-phase is the sponge phase. To the right the same diagram is shown on linear scale and more schematically [5]. The abbreviations for the different phases are discussed in the text below (see also Table 2).*

lamellae are relatively well ordered due to steric interactions. Steric interactions are typical for non-ionic surfactants, which do not possess a Coulomb interaction. For ionic surfactants the lamellar phase is formed at lower concentrations due to the strong interaction. Astonishingly, more ordered phases appear. The H_1-phase contains cylindrical micelles (as the L_1-phase), but the cylinders are ordered on a hexagonal lattice. Again, the steric repulsion is sufficient to order the micelles in a liquid crystalline state. The V_1-phase has a cubic unit cell, while the hydrophilic and hydrophobic domains are continuous in the whole volume. This phase is also called 'plumbers nightmare' because the high viscosity might result in plugging of tubes. The exact structure will be discussed in the text below. We see that liquid crystalline phases (L_α, H_1, V_1) exist with liquid crystalline order. These phases are also termed lyotropic because the addition of water is responsible for the formation. So this term arises from the viewpoint of the solid phase S, which means mainly a pure surfactant with small impurities of water.

In Fig. 3 there are also two-phase regions marked. In this region two phases coexist, so either the sample gets turbid because of many small domains or, after a long time, the sample forms a meniscus between the two clear phases. The horizontal lines indicate the corresponding coexisting phases, so from a given overall concentration one follows the tie-lines to the right and left, and reads off the properties of the coexisting phases. The lines are horizontal, because the vertical axis is the temperature. For more complicated phase diagrams (we shall see later) the tie lines can be tilted. The example $L_3 + W$ or $L_1 + L_3$ indicates a coexistence of the sponge phase L_3 with a highly water rich phase. The example $L_1' + L_2''$ or 2Φ indicates two coexist-

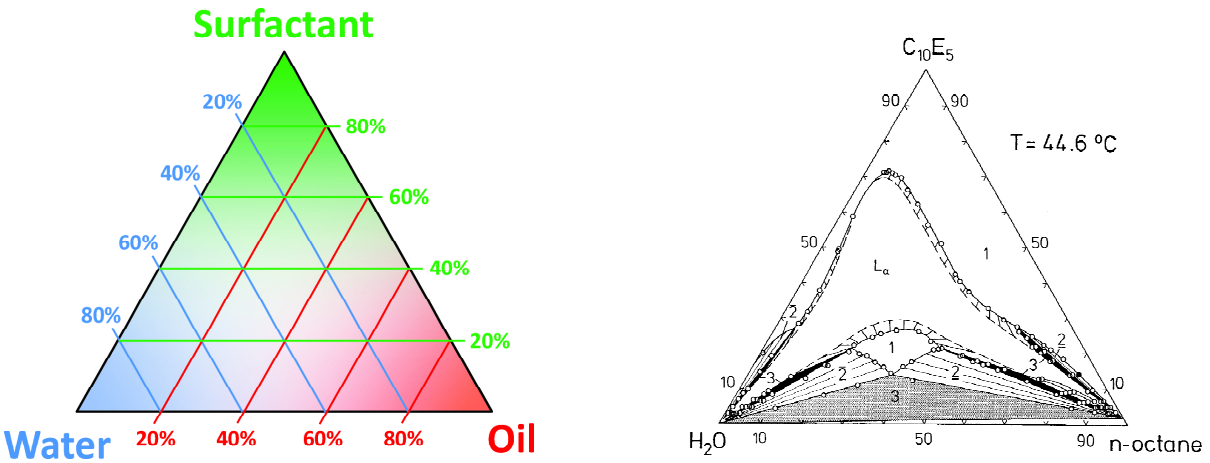

Fig. 4: *Left: A scheme how to read off the compositions from the Gibbs Phase Triangle. The axis to the left of the corresponding component in the corner shows the scale of the fraction. The colored lines indicate constant composition. The whole diagram is completely symmetric. Right: A rather simple phase diagram for the system: H_2O, n-octane, $C_{10}E_4$ [7]. The numbers inside indicate the number of phases, and L_α indicates the lamellar phase.*

ing micellar phases. One of them contains spherical and the other one cylindrical or wormlike micelles.

In summary for the aqueous surfactant systems the following points shall be clear. The CMC separates the highly diluted from the diluted region. The entropy favors unimeric surfactant molecules while the enthalpy favors micelles. The concept of packing explains the micellar shapes. These shapes have a high degree of symmetry, because each surfactant molecule is identical. The shapes range from spherical over cylindrical to lamellar. At higher concentrations, the interactions between the micelles lead to lyotropic (or liquid crystalline) phases. There exist phases with the same micellar shapes of the diluted region, but also ordered phases with new unit cells (see V_1). The interactions are sterically repulsive for non-ionic surfactants and Coulomb-like for ionic surfactants. Theoretical concepts of the interactions will be given in the following chapter. The parameter temperature comes into play here because enthalpic and entropic contributions are weighted differently.

3 Microemulsions

So far we have been focusing on two-phase systems. For cleaning processes the uptake of oil is an important issue. Then microemulsions will be formed. It is known that on a microscopic level there are domains of (nearly) pure water and oil, and the surfactant is at the interface. In this sense, the surfactant mediates between the hydrophilic and hydrophobic components, which leads to macroscopically homogenous fluids. Thus, microemulsions are mostly optically clear, which is one criterion for phase diagram measurements.

A rather simple phase diagram is shown in Fig. 4. There are now one-phase, two-phase, and three-phase coexistence regions, since now three components are used. The most interesting region is the small one-phase region almost in the center of the phase triangle. Here the bicontinuous microemulsion is found. The components oil and water both form a sponge-like structure, i.e. each of the sponge hosts the other one. In this sense the phase is *bi*-continuous

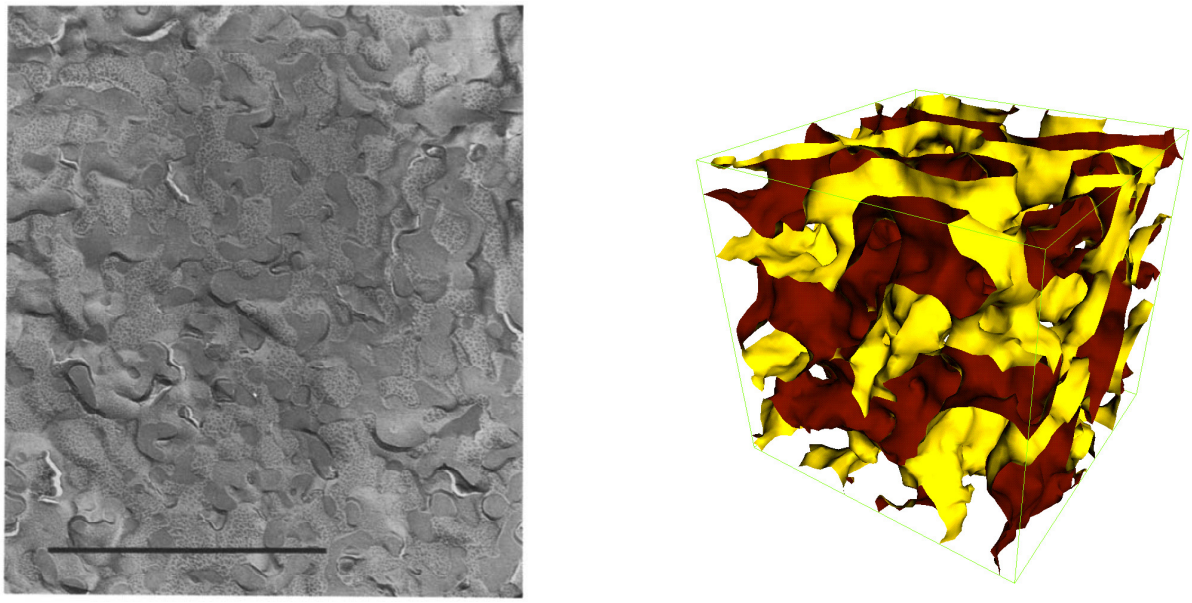

Fig. 5: *Left: A transmission electron micrograph of the microemulsion containing water, octane, and $C_{12}E_5$. The surfactant content was 7 wt% (see Ref. [8]). The indicated bar shows a scale of 1μm. Right: A real space picture of the bicontinuous microemulsion according to computer simulations [9]. Actually the surfactant film is shown with the surface color being red for oil facing surface and yellow for water facing surface.*

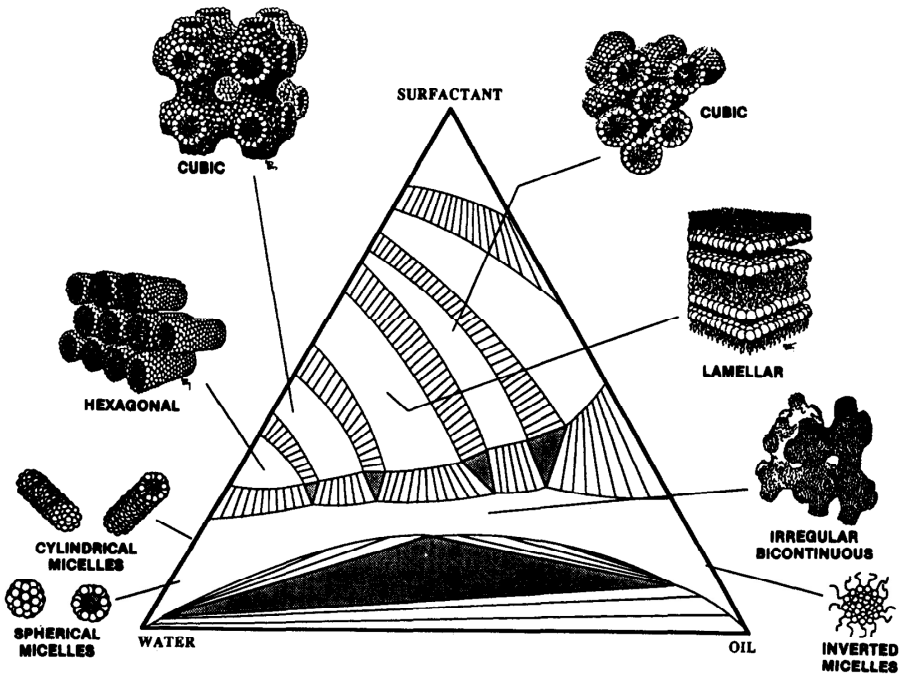

Fig. 6: *A more schematic phase triangle with most typical lyotropic phases [10]. At the bottom there is the three-phase coexistence region (black) surrounded by two-phase coexistence regions. Above there is the large L_1-region with droplets, cylinders and the bicontinuous phase. In the upper half there are many lyotropic phases such as the hexagonal H_1, the cubic V_1, the lamellar L_α, and the fcc or bcc cubic I_1 phase.*

(see also Fig. 5). This can for instance be proven by conductivity measurements. The grey three phase coexistence region in the bottom of the triangle indicates a coexistence of a water-rich, an oil-rich, and a bicontinuous phase. Here the concept of tie-lines breaks down. Contrarily, all two-phase regions are filled with tie-lines, which are tilted now. At very low surfactant concentrations the droplet phase is found. This phase is nearly invisible on the current scale. A more schematic phase diagram with lyotropic phases is depicted in Fig. 6. One important point is the large L_1 phase where droplets, cylinders, and the bicontinuous phase are included. Entropic contributions destroy clear phase transitions between the distinct structures, and so coexistence is possible. On the bottom right the reversed micelles are found. Another point of this scheme is the indication the most important lyotropic phases. Their real space pictures are indicated around the phase triangle. The structures show closed micelles with the hydrophobic component inside. In principle, the reversed micelles are possible as well. After we have seen that different authors use different abbreviations for the same phases a list of all possible abbreviations should be given. A first attempt was made by Tiddy [11] that we now extend for our own purposes (see Table 2).

While the theoretical concept for aqueous surfactant systems describes the micelles as bulky objects the most widely accepted concept for microemulsions bases on the theory of Helfrich [13]. Here it is assumed that the surfactant forms a membrane and the free energy of the overall system is dominated by the elastic properties of the membrane. The free energy reads then:

$$F = \int dS \left(\gamma + \frac{1}{2}\kappa(c_1 + c_2 - 2c_0)^2 + \bar{\kappa} c_1 c_2 \right) \tag{2}$$

The first addend describes the surface tension of the membrane. In principle the surfactant might vary the formed surface by different tilt angles (the molecules are not oriented perpendicular) or by crystallization of the hydrophobic tails. For our purposes we assume a liquid membrane, and neglect variations of the overall surface. The next summand is a product of the bending rigidity κ and the deviation of the mean curvature $\frac{1}{2}(c_1 + c_2)$ from the equilibrium curvature c_0. The curvature arises from a tangential construction at a given membrane point (see Fig. 7). Namely, two perpendicular circles describe the tangent. Their reciprocal radius is the curvature, i.e. $c_i = R_i^{-1}$. A positive curvature means a curvature towards the oil domain. The middle summand is sensitive to deviations of the mean curvature from the equilibrium curvature. The last addend is a product of the saddle splay modulus $\bar{\kappa}$ and the Gaussian curvature $c_1 c_2$. A saddle shape for instance has a negative Gaussian curvature, while for a sphere the Gaussian curvature is positive, i.e. $c_1 c_2 = R^{-2}$. One finds typical values of $\kappa \approx 1..10 \mathrm{k}_B\mathrm{T}$ and $\bar{\kappa} \approx -\kappa$ for soft to rigid membranes. On this basis predictions for the phase behavior can be made as we will see below.

The first problem to tackle is the L_1 phase. As we have seen, there exist spherical and cylindrical micelles. The lamellar phase L_α will be taken into account as well. The problem was treated by Safran [14] for the first time by comparing the free energies for the three different cases. Since the bodies were assumed to be ideally shaped the calculations were kept quite simple. He found that the three different shapes are separated by distinct phases. The same problem was described by Blokhuis [15] in a slightly extended way: Emulsification failure and coexistence of the two micelle types was taken into account. The results are shown in Fig. 8. On the y-axis the dimensionless ω/R_0 is used. It bases on the ratio of the toal volume and the total membrane area, i.e. $\omega = V_{\mathrm{tot}}/S_{\mathrm{tot}}$, and the equilibrium radius $R_0 = c_0^{-1}$. The x-axis is spanned by the ratio of the two moduli $\bar{\kappa}/\kappa$. From small to large surfactant concentrations one passes from the two phase coexistence ($\bar{2}\varphi$) over the micellar shapes (spheres/cylinders) to the lamellar phase.

Table 2: *A survey about symbols for the different phases in aqueous surfactant systems and microemulsions. A first attempt was introduced by Tiddy [11]. Especially more exotic examples are given there. The second column gives symbols for polymeric systems [12], which will be discussed in a later section.*

symbol used here	symbol (polymers)	alternative symbols	explanation
1, 1Φ		L_1 or L_2	micelles & fluctuating bicontinuous phase
2, 2Φ		$L_1' + L_1''$, ...	2 coexisting phases (need to be specified)
$\bar{2}$, $\underline{2}$			2 coexisting phases at high/low temperatures
3, 3Φ		$L_1 + L_2 + L_3$, ...	3 coexisting phases (need to be specified)
L_1	M_1		micelles, hydrophopic part inside
L_2	M_2		reversed micelles, hydrophilic part inside
L_3			bicontinuous phase
L_α	L	D, G	lamellar phase, ordered
H_1	H_1	E, H_I, M_1	hexagonal phase, ordered
H_2	H_2	F, H_{II}, M_2	reversed hexagonal phase, ordered
I_1	C_1	Q_I, S_{1c}	cubic phase$_{\mathrm{fcc,bcc}}$ with spherical micelles
I_2	C_2	Q_{II}	cubic phase$_{\mathrm{fcc,bcc}}$ with rev. spher. micelles
V_1		I_1', Q_I	cubic phase with bicontinuous structure
V_2		I_2', Q_{II}	cubic phase with rev. bicont. structure
	G_1		cubic gyroid phase
	G_2		cubic gyroid phase, reversed

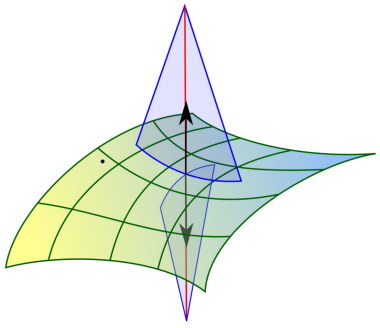

Fig. 7: *An example of a surface with the two principal radii indicated. This construction can be done for any point of the surface.*

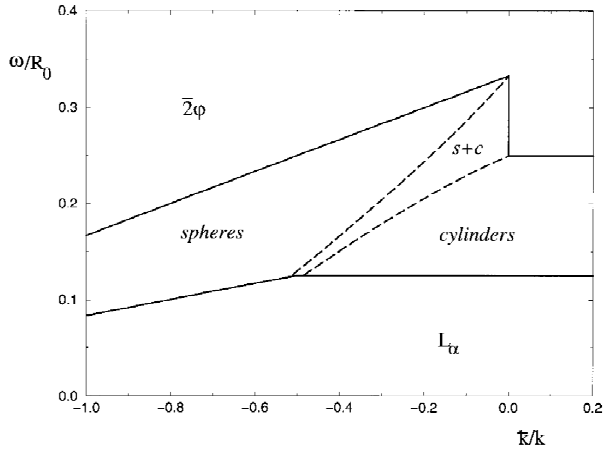

Fig. 8: *Microemulsion phase diagram [15]. The parameter ω/R_0 is given by the ratio of the total volume and the membrane surface and the equilibrium curvature, i.e. $\omega/R_0 = V_{\mathrm{tot}}/S_{\mathrm{tot}} \cdot c_0$. The x-axis shows the ratio of the two moduli $\bar{\kappa}/\kappa$.*

The choice of the micellar shape is driven by the ratio of $\bar{\kappa}/\kappa$. This means if $\bar{\kappa}$ is strongly negative the spherical micelles are favored. Cylinders (with no Gaussian curvature) are favored from slightly negative to positive $\bar{\kappa}$-values. The theory of Blockhuis was extended to include the translational entropy and polydispersity of the geometrical dimensions. This example shows nicely that entropy smears out the transition between spherical and cylindrical micelles. At this stage of the theory the micelles do not interact.

The interactions to be considered are either sterically repulsive or long ranged Coulomb interactions. The treatment usually involves approximations in different ways. We will introduce two different methods in this manuscript. Schwarz and Gompper [16, 17] considered different minimal surfaces on a cubic lattice. The principal structures are known already (see Fig. 9). For such surfaces the elastic energy as given in equation 2 is minimal with respect to the boundary conditions. In principle, such surfaces were also used as decorative architecture, for instance for the Olympic stadion in Munich. They can be understood as soap bubbles, which form the shape due to the surrounding (boundary condition) and the surface tension. The different minimal surface energies of the cubic symmetry need to be calculated and compared for the different structures. Interestingly, thermal fluctuations can approximately be taken into account. The additional free energy term reads then:

$$F_{\mathrm{steric}} \propto c_0^{-2} \left(\frac{k_B T}{\kappa}\right)^2 \frac{\phi_{\mathrm{oil}}^3}{(1-\phi_{\mathrm{oil}})^2} \tag{3}$$

This energy depends on the bending rigidity κ and the oil volume fraction ϕ_{oil}. For large κ the fluctuations are suppressed, and the additional free energy becomes small. Small equilibrium curvatures c_0 and large oil fractions ϕ_{oil} may make the steric term large. The result of this calculations is that the cubic structures *G*, *D*, and *P* are favored with respect to the other cubic structures taken into account (see Fig. 9).

Another approach bases on a Landau expansion. For this purpose the order parameter Φ needs to be defined. Inside the whole sample the function $\Phi(r)$ takes values between -1 and $+1$. The extreme cases indicate pure oil and pure water domains. Since the function is continuous intermediate values exist in between. These values are usually interpreted as the presence of surfactant. Pure surfactant would mean $\Phi = 0$ while intermediate values are interpreted as mixtures of oil or water with the surfactant. This modelling is contradicting in two aspects: First, the domains of oil and water have usually sharp boundaries and the order parameter would be discontinuous. Second, the nearly incompressible fluid would actually need two order parameters to describe the physics completely. For simplicity reasons and due to its success, the simple model is still often used in the literature [18]. Generally, the Landau approach is very successful in describing fluctuations and phase transitions in solid state physics, soft matter physics and more remote fields. The free energy functional was kept dimensionless in reference [18], and it reads:

$$F[\Phi] = \int dV \left(-\frac{\chi}{2}\Phi^2 + \frac{1-\Phi}{2}\ln\frac{1-\Phi}{2} + \frac{1+\Phi}{2}\ln\frac{1+\Phi}{2} - \frac{1}{2}(\nabla\Phi)^2 + \frac{1}{2}(\nabla^2\Phi)^2 - \mu\Phi\right) \tag{4}$$

The first addend is a simplified treatment of interactions on the basis of a point like interaction with the interaction parameter χ. It is fully correct for steric repulsions, and also for polymeric systems with only next neighbor interactions. Coulomb interactions would need a distance dependent interaction. The next two terms arise from the translational entropy of the oil and water

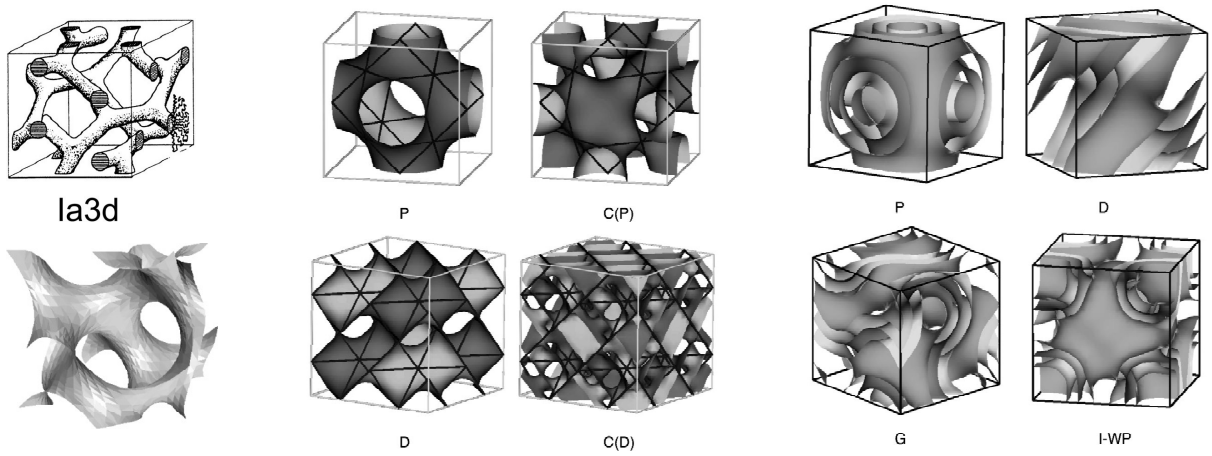

Fig. 9: *Left: The most prominent structure: The gyroid phase G (G_1). Middle: The next most prominent structures in a cubic phase. Especially the D and P (V_1) are realized. Right: Double frequency structures. These structures are not realized often. Graphs from [16, 17].*

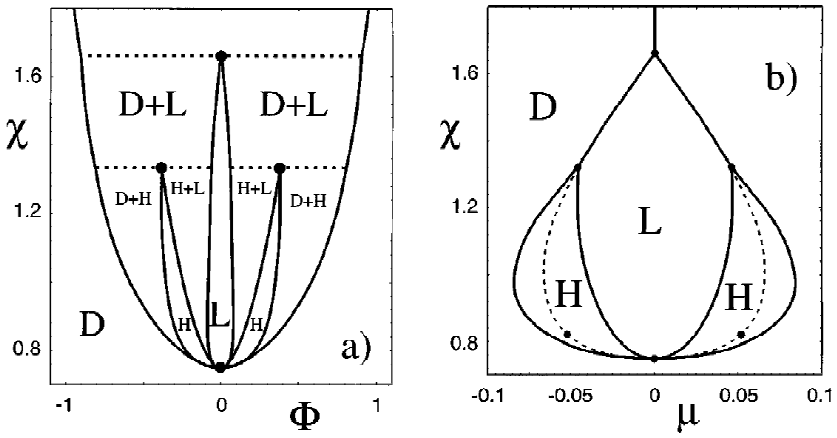

Fig. 10: *Two-dimensional bulk phase diagram [18], showing disordered (D), lamellar (L), and hexagonal (H) phases, as a function of the interaction parameter χ. The x-axis is spanned by (a) the average order parameter $\Phi = -1 + 2\phi_{\mathrm{oil}}$, and (b) the chemical potential μ. Dashed lines in (a) denote triple lines and dashed lines in (b) denote the (metastable) L-D transitions, which exhibit tricritical points (denoted by solid circles).*

domains (The size of the molecules is assumed to be identical). Actually, these two terms do not follow strictly the concept of a Landau approach, because then only a Taylor expansion of this expression would appear. The next two terms arise from the functional expansion of the order parameter. Odd terms do not appear due to the high symmetry of the system (usually assumed; for instance a gradient term could describe gravity effects). The gradient term describes the low surface tension of the system. The negative sign means that certain surfaces between domains are favored (especially on large length scales). The next order correction sets a limit to these surfaces (at small length scales the homogenous state is favored). The last term describes the chemical potential describing the conjugated field [19]. In this way the phase diagram can be displayed as a function of the mean order parameter or the conjugated field. The direct prediction is the existence of lamellar L_α and hexagonal H_1 and H_2 fields (see Fig. 10). For such a phase diagram either different ordered fields $\Phi(r)$ with sinusodial oscillations are assumed analytically and their free energy is compared on the basis of the integral (eq. 4). A better approach is obtained by computer calculations of $\Phi(r)$ on a lattice. The computer can take higher order oscillations into account more easily. Furthermore, a computer can simulate thermal fluctuations relatively straight forward, while analytically the effort is often relatively high, especially for the ordered phases. The left diagram (Fig. 10a) shows the phase diagram as a function of a scaled reciprocal temperature (i.e. the interaction parameter χ and the composition $\Phi = -1 + 2\phi_{\text{oil}}$. There are different regions indicated by D for disordered, L for lamellar, and H for hexagonal, and further coexistence regions. This phase diagram has a prominent disordered region, which would mean that oil and water do not form separated domains. For polymers this is possible as we will see later in the manuscript. For microemulsions the interaction parameter would be rather large such that mainly ordered phases exist, at least in this sense that oil and water domains are formed. Equation 4 is quite oversimplified to describe the complex behavior of microemulsions. So there exist more detailed approximations (see Ref. [20, 21]), which aim at better descriptions, but on the other hand the more complicated algebra cannot be discussed in this manuscript. It should be mentioned that Ref. [21] treats Coulomb interactions quite explicitly.

4 Phase Diagram Measurements

Optical measurements base on different observations: Turbidity, meniscus, and depolarization. Turbidity indicates a two- or three-phase coexistence, which is a quickly obtained criterion. The observation of the meniscus after long waiting times allows to determine the ratio of the volumes precisely. This is for instance helpful to determine the three-phase coexistence boundary (see Fig. 4). By changing the composition (or temperature) and following the minority phase to vanish the boundary to the two-phase coexistence is extrapolated. When observing a one-phase sample with crossed polarizers one finds some phases, which depolarize the light while most of the phases keep the polarization. The reason for depolarization is elongated domains, which give rise to different propagation for different polarizations. Because most of the samples are 'powder-like', i.e. with many grains, the light is simply depolarized. Elongated domains are found for the hexagonal phases H_1 and H_2, and for the lamellar phase. Please note that cubic phases are isotropic and do not give rise to depolarization. Another, not really optic criterion is also the viscosity. By shaking the sample tube, one gets rough information about the viscosity and thus can speculate about the ordered phases.

The real scientific field behind viscosity is *Rheology* (see also Chapter A7). Usually, the sample

is placed between two plates. One of the plates is oscillating either elongationally or rotationally with relatively small excitations. For rotations the plates do not need to be parallel. One plate is often conical to have the same shear for all radii. The still plate takes up the force. There the amplitude and phase shift is measured with respect to the moving plate. In most cases the amplitude is used to characterize the different phases. This method is rather indirect because the absolute values often do not tell the difference. But it is plausible that lamellar phases and hexagonal cylinder phases allow the domains to slide with small losses while cubic phases are rather rigid. The L_1 and L_3 phase usually show the lowest viscosity. Low temperatures can lead to rather rigid phases in parallel simply by raising the viscosity of oil and water.
Another method often used is *nuclear magnetic resonance* (NMR, see also Chapter A2). Mostly the isotropic phases are distinguished from the phases with elongated domains [22]. The anisotropic phases show a quadrupolar splitting of an otherwise single line. Some more examples for NMR measurements are given in Ref. [11]. Please note that the CMC can also be determined by NMR [2] as mentioned before.

4.1 Scattering Methods

By small angle neutron and x-ray scattering one can distinguish ordered phases quite well (see also Chapter A3). With neutrons limited resolution often does not allow to distinguish all higher order peaks. This is why x-rays are most often preferred. The principle behind this method is powder diffraction because usually the domains are not oriented and so many grains with different orientation coexist. Especially, cubic phases cannot be ordered by external fields. So, Debye-Scherrer rings are observed on a 2-dimensional detector. After averaging the intensities on concentric circles the intensity is simply shown as a function of the modulus of the scattering vector q. The observed peaks are indexed according to multiples of the q-value with respect to the first peak with the lowest q. These are either square roots of natural numbers or of simple fractions. In Soft Matter research these ratios are simply used as labels for the peaks instead of the full information of the Miller indices (h, k, l). Nonetheless, the experimentalist needs to know the crystallography [23] behind in order to exclude some ratios, which do not exist. In Table 3 many important examples are shown.
The lamellar phase expands in two dimensions and the periodicity usually extends in z-direction (with a distance d). The reciprocal lattice is periodic in z as well. The distances are given by $q = 2\pi/d$. In reciprocal space the lattice is formed by delta-function like peaks. In x, y-direction it arises from the infinite dimensions, and in z the strict periodicity is the reason.
The hexagonal phase consists of infinitely long cylinders (or rods) in z-direction, while in the x, y-plane the structure is periodic. The reciprocal structure is periodic in x, y (note: the lattice is turned by 60°) while the delta-like peaks do not expand in z-direction. The number of peaks with the same distance from the origin can be counted according to $n_{h,k,l} = 12$ for $h > k > 0$ and $n_{h,k,l} = 6$ otherwise. This frequency has to be taken into account for the intensities of the Debye-Scherrer rings.
For the cubic structures the following shall be mentioned: The simple cubic (sc) lattice stays simple cubic in reciprocal space. The body centered cubic (bcc) lattice becomes a face centered cubic (fcc) lattice and vice versa. The gyroid phase is presented as a more exotic phase [24]. The number of peaks of the cubic lattices can be counted according to $n_{h,k,l} = 2^s \cdot c$, where s counts the number of h, k, l different from zero (so here the sign matters), and c is a combinatorial factor being 1 for $h = k = l$, 3 for $h \neq k = l$, and 6 for $h \neq k \neq l$.
The nomenclature I_1 for the cubic phase is often quite sloppy. The name actually arises only

Table 3: *Most important ordered structures. The reciprocal space structure consists always of delta-like peaks and can be taken as a structure factor; then the real space structure is assumed to be infinitely thin. The lattice points of reciprocal space are given by Miller indices and are sorted by vector length (as given in the third column). Colored dots give connection to Miller indices; the origin is always indicated by a black dot.*

real space	reciprocal space	lattice points of reciprocal space (Miller indices)		
lamellar 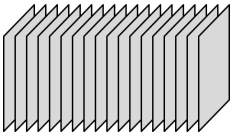	(lamellar) 	$(h,0,0)$		
		$(1,0,0)$ 1 $(2,0,0)$ 2 $(3,0,0)$ 3 $(4,0,0)$ 4	$(5,0,0)$ 5 $(6,0,0)$ 6 $(7,0,0)$ 7 $(8,0,0)$ 8	$(9,0,0)$ 9 $(10,0,0)$ 10 $(11,0,0)$ 11 ...
hexagonal 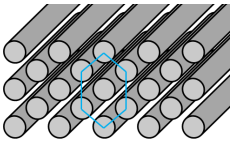	hexagonal 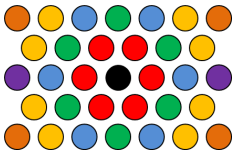	$(h,k,0)$		
		$(1,0,0)$ 1 $(1,1,0)$ $\sqrt{3}$ $(2,0,0)$ $\sqrt{4}$ $(2,1,0)$ $\sqrt{7}$ $(3,0,0)$ $\sqrt{9}$	$(2,2,0)$ $\sqrt{12}$ $(3,1,0)$ $\sqrt{13}$ $(4,0,0)$ $\sqrt{16}$ $(3,2,0)$ $\sqrt{19}$ $(4,1,0)$ $\sqrt{21}$	$(3,3,0)$ $\sqrt{21}$ $(5,0,0)$ $\sqrt{25}$ $(4,2,0)$ $\sqrt{28}$ $(5,1,0)$ $\sqrt{31}$ $(4,3,0)$ $\sqrt{31}$
sc 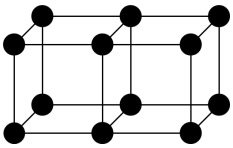	sc 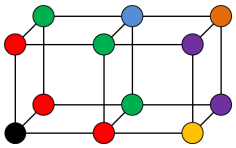	(h,k,l)		
		$(1,0,0)$ 1 $(1,1,0)$ $\sqrt{2}$ $(1,1,1)$ $\sqrt{3}$ $(2,0,0)$ $\sqrt{4}$ $(2,1,0)$ $\sqrt{5}$	$(2,1,1)$ $\sqrt{6}$ $(2,2,0)$ $\sqrt{8}$ $(2,2,1)$ $\sqrt{9}$ $(3,0,0)$ $\sqrt{9}$ $(3,1,0)$ $\sqrt{10}$	$(3,1,1)$ $\sqrt{11}$ $(2,2,2)$ $\sqrt{12}$ $(3,2,0)$ $\sqrt{13}$ ...
bcc 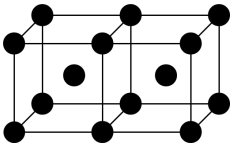	fcc 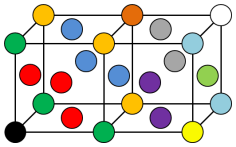	(h,k,l) and $(h+\frac{1}{2},k+\frac{1}{2},l)$		
		$(\frac{1}{2},\frac{1}{2},0)$ $\sqrt{\frac{1}{2}}$ $(1,0,0)$ $\sqrt{1}$ $(1,\frac{1}{2},\frac{1}{2})$ $\sqrt{\frac{3}{2}}$ $(1,1,0)$ $\sqrt{2}$ $(\frac{3}{2},\frac{1}{2},0)$ $\sqrt{\frac{5}{2}}$	$(1,1,1)$ $\sqrt{3}$ $(\frac{3}{2},1,\frac{1}{2})$ $\sqrt{\frac{7}{2}}$ $(2,0,0)$ $\sqrt{4}$ $(2,\frac{1}{2},\frac{1}{2})$ $\sqrt{\frac{9}{2}}$ $(\frac{3}{2},\frac{3}{2},0)$ $\sqrt{\frac{9}{2}}$	$(2,1,0)$ $\sqrt{5}$ $(2,\frac{3}{2},\frac{1}{2})$ $\sqrt{\frac{13}{2}}$ $(\frac{5}{2},\frac{1}{2},0)$ $\sqrt{\frac{13}{2}}$ ...
fcc 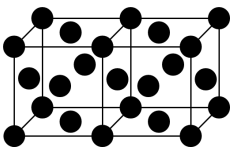	bcc 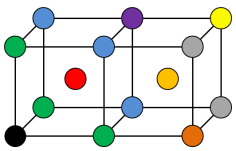	(h,k,l) and $(h+\frac{1}{2},k+\frac{1}{2},l+\frac{1}{2})$		
		$(\frac{1}{2},\frac{1}{2},\frac{1}{2})$ $\sqrt{\frac{3}{4}}$ $(1,0,0)$ $\sqrt{1}$ $(1,1,0)$ $\sqrt{2}$ $(\frac{3}{2},\frac{1}{2},\frac{1}{2})$ $\sqrt{\frac{11}{4}}$ $(1,1,1)$ $\sqrt{3}$	$(2,0,0)$ $\sqrt{4}$ $(\frac{3}{2},\frac{3}{2},\frac{1}{2})$ $\sqrt{\frac{19}{4}}$ $(2,1,0)$ $\sqrt{5}$ $(2,1,1)$ $\sqrt{6}$ $(\frac{5}{2},\frac{1}{2},\frac{1}{2})$ $\sqrt{\frac{27}{4}}$	$(\frac{3}{2},\frac{3}{2},\frac{3}{2})$ $\sqrt{\frac{27}{4}}$ $(2,2,0)$ $\sqrt{8}$ $(\frac{5}{2},\frac{3}{2},\frac{1}{2})$ $\sqrt{\frac{35}{4}}$ ...
gyroid Ia$\bar{3}$d 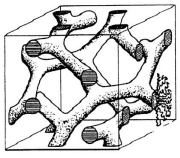	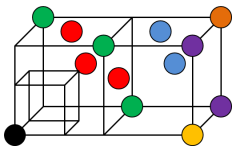	$(h,k,0)$ with $h+k+l=2n$ and further restrictions		
		$(2,1,1)$ $\sqrt{6}$ $(2,2,0)$ $\sqrt{8}$ $(3,2,1)$ $\sqrt{14}$ $(4,0,0)$ $\sqrt{16}$ $(4,2,0)$ $\sqrt{20}$	$(3,3,2)$ $\sqrt{22}$ $(4,2,2)$ $\sqrt{24}$ $(4,3,1)$ $\sqrt{26}$ $(5,2,1)$ $\sqrt{30}$ $(4,4,0)$ $\sqrt{32}$	$(6,1,1)$ $\sqrt{38}$ $(5,3,2)$ $\sqrt{38}$ $(6,2,0)$ $\sqrt{40}$ $(5,4,1)$ $\sqrt{42}$ ...

Table 4: *Form factors in connection with the liquid crystalline structures discussed in Table 3. The lamellar structure factor arises from a 1-dim, the cylindrical from a 2-dim, and the spherical from a 3-dimensional calculation. J_1 is the Bessel function of first kind and first order. d indicates the lamellar domain thickness, and r the radius of the cylinder and the sphere.*

lamellar	$F(q) = \left(\frac{\sin(qd/2)}{qd/2}\right)^2$
cylindrical	$F(q) = \left(2\frac{J_1(qr)}{qr}\right)^2$
spherical	$F(q) = \left(3\frac{\sin(qr) - qr\cos(qr)}{(qr)^3}\right)^2$

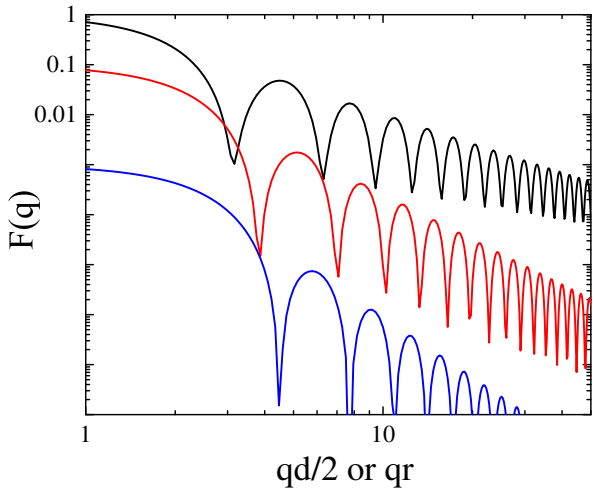

Fig. 11: *Double logarithmic plots of the form factors $F(q)$ for lamellae (black), cylinders (red), and spheres (blue). For a clear representation the curves are shifted down by a factor of 1, 0.1 and 0.001. The original functions are normalized to 1 for $q \to 0$.*

from the word isotropic but the actual structure behind can be simple cubic, body or face centered cubic. One publication [25] demonstrates this problem for even more complicated cubic structures. Furthermore, Brownian motion – as for microemulsions – can destroy the long range order and so only fluid-like near-order is achieved. This is usually expressed in missing higher order peaks, and no crystal-like order can be determined. Contrarily, the gyroid phase is usually well distinguished from the cubic phase with globular domains, but this phase only appears for polymer based systems.

For indexing the Debye-Scherrer rings Table 3 gives a good basis. So there are many examples in the literature, which argue mainly on the basis of the appearing peaks [12]. For a quick reference this technique might be sufficient. Nonetheless, the analysis can go one step beyond if a model is assumed for the 3-dimensional structure of the domains. This means, that the lamellae have finite thickness, the cylinders have a finite diameter, and the spherical domains on the cubic lattice have a finite diameter. For such structures one then splits the problem in two parts: The periodic structure is given by Table 3, while the single domain is described by a form factor.

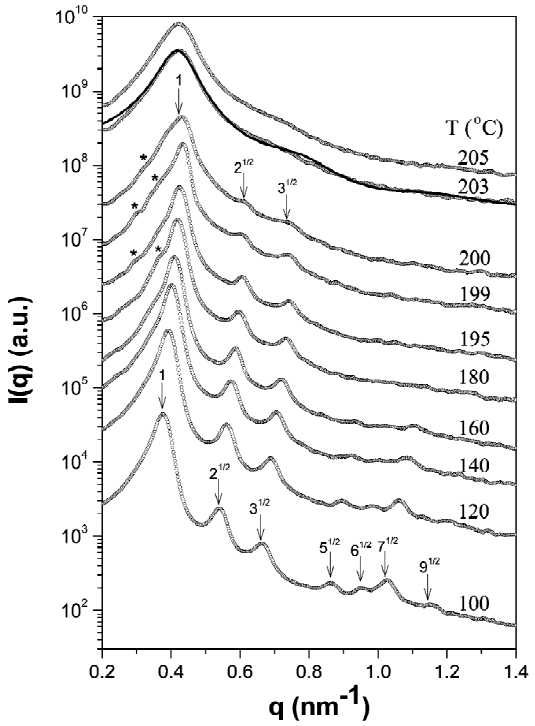

Fig. 12: *In this example small angle x-ray scattering curves $I(q)$ are shown as a function of temperature [29]. For different temperatures different factors scale the curves down for better visibility. At the lowest temperature (100°C) the order is developed best, and many peaks indicate the face centered cubic order of spherical entities. The numbers give the ratios of the peak q-values.*

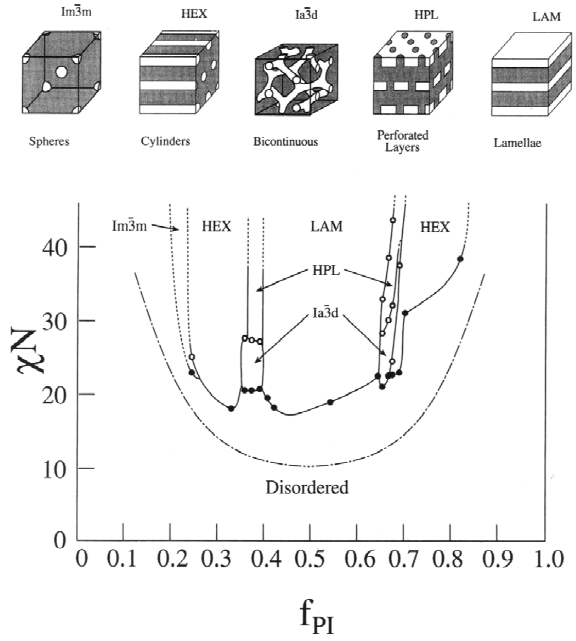

Fig. 13: *Experimental phase diagram of a diblock copolymer melt [30]. The substance is polystyrene-polyisoprene (PS-PI). The y-axis shows the scaled interaction parameter χ; the x-axis shows the chain length ratio f_{PI}. The ordered phases are indicated as LAM for lamellar (L_α), Ia$\bar{3}$d for gyroid (G_1 and G_2), HEX for hexagonal (H_1 and H_2), and Im$\bar{3}$m for the body centered cubic phase (I_1 and I_2). The hexagonally perforated lamellar structure (HPL) is not found consistently for all polymers. All structures are also displayed in sketches above.*

$$I(q_{h,k,l}) \propto S(q_{h,k,l}) \cdot F(q_{h,k,l}) \tag{5}$$

In this equation the structure factor $S(q)$ arises from the delta-function peaks of the reciprocal lattice. The form factor $F(q)$ is connected with the 3-dimensional structure of the single domain. Very often, equation 5 can be simplified to an orientationally averaged form according to:

$$I_{\mathrm{av}}(q) \propto \frac{1}{q^2} \cdot \sum_{q_{h,k,l}=q} n_{h,k,l} \cdot F(q) \tag{6}$$

Table 4 gives a list of form factors for differently shaped domains. The functions are plotted in Fig. 11. It becomes clear now that zeros of the formfactor might result in further eliminations of Debye-Scherrer rings. So the full list of Bragg peaks gives the maximum set of peaks, and the exact form factor might cause further eliminations, which can be interpreted as a higher degree of symmetry.

A very good example for peak indexing is discussed now in context with Fig. 12. The system is a polybutadiene-polyethyleneoxide (PB(1,4)-PEO) diblock copolymer in a melt. The phase separation leads to spherical domains of PEO hosted in the PB matrix. At high temperatures (203°C) the spherical domains show only a near order. The repulsive interactions are modeled by a Perkus-Yevic structure factor (excluded volume interaction). Upon lowering the temperature the liquid crystalline order becomes more prominent, which is indicated by a larger number of higher order peaks. Finally, at 100°C the best order is achieved, and the highest order visible is found at a relative q value of $\sqrt{9}$.

It shall be mentioned that at this stage of the theory all thermal fluctuations are neglected. Fluctuations will lead to undulations of the domain surface. This can lead to suppression of higher order Bragg peaks. For instance for the lamellar order of a surfactant film or bilayer the theory of Caillé describes the scattering. A good review can be found in Ref. [26] and further developments in Ref. [27]. A simpler approximation for undulations of a domain surface can be achieved by a multiplication of a Gaussian to equation 6. Another form of disorder is obtained by non-perfect repetitions of the crystalline order. Then the paracrystal model [28] needs to be taken into account. The result is broader Bragg peaks for the higher orders with lower peak intensities. So any kind of disorder leads to weaker higher order Bragg peaks. It shall be mentioned that the Caillé theory actually includes both ways of disorder.

5 Polymer-Based Microemulsions

Diblock copolymers are relatively similar to amphiphilic molecules. They are long chain molecules with two different ends. The interactions between the chemically different parts can be understood on the basis of segments. Very often, the different segments are not well miscible, but the interactions are much weaker as for amphiphiles. The chain length is responsible for the multiplication of individually interacting segments, such that the two blocks tend to phase separation. This phase separation happens for the pure diblock copolymer melt, and leads to ordered domains. In Fig. 13 a phase diagram of the polymer polystyrene-polyisoprene (PS-PI) is shown. On the vertical axis the scaled interaction paramter χ is shown. It has the temperature dependence $\chi = \chi_h/T + \chi_s$ with an enthalpic and entropic contribution. So high temperatures are indicated by small χ and vice versa. The scaling with the segment number N is done because the observed phases do not always lie in the accessible temperature range, and so one has to investigate different molar masses. The horizontal axis shows the chain length ratio f_{PI}, which is the ratio of the molar masses of both blocks ($f_{\mathrm{PI}} = m_{\mathrm{PI}}/(m_{\mathrm{PS}}+m_{\mathrm{PI}})$). This phase diagram can be well compared to the theoretical phase diagram of Fig. 10a (with $\Phi \sim f$). At high temperatures (low χ) the diblock copolymer is disordered. Here the interactions between the different segments are favorable enough that no domains are formed. At low temperatures different ordered phases are found. Experimentally, there is the lamellar phase in the center; the gyroid phase in the direct neighborhood (the perforated layers shall be neglected); then there is the hexagonal phase, and finally the body centered cubic phase. The simple theory of Fig. 10a only finds the lamellar and hexagonal phase, and – more important – some relatively large areas of phase coexistence, but more precise theories about polymer melts are well capable of describing the experimental phase diagrams much closer. The general layout of the phase diagram is the same. So the order of different phases is found from the center to the outer regions relatively symmetrically. Of course, the domain structure is inverted to higher f_{PI} with respect to lower f_{PI}. Extreme concentrations f_{PI} close to 0 or 1 are mainly dominated by the disordered

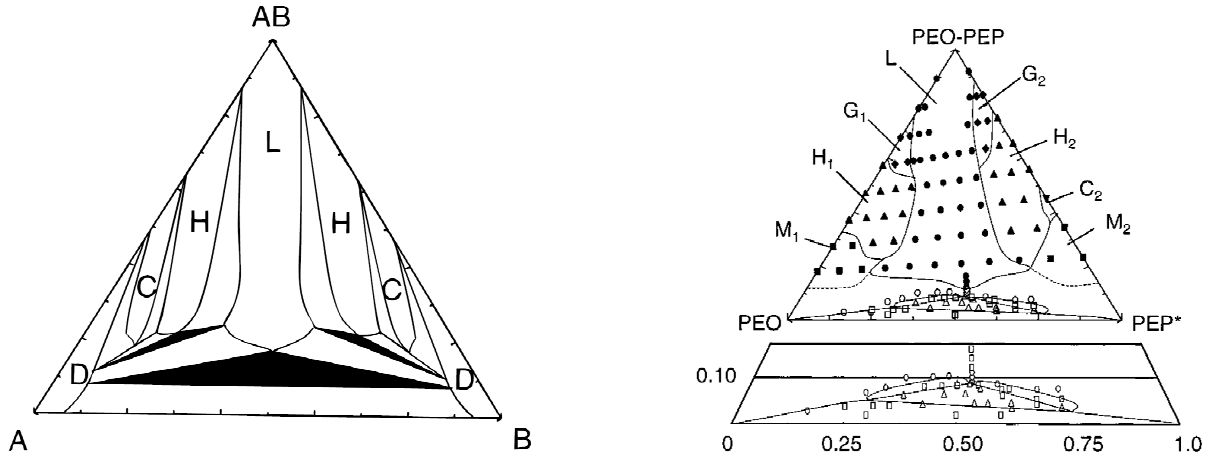

Fig. 14: *Left: A theoretical phase diagram [12] from a simple theory (a mean field theory resulting in equations similar to eq. 4). A lamellar, two hexagonal, two cubic and two disordered phases are predicted. Coexistence regions are in between (white), and three phase coexistence is indicated in black. Right: An experimental phase diagram from the system PEO/PEP/PEP-PEO [12]. Interestingly, a highly symmetric diagram with lamellar (L), gyroid (G_i), hexagonal (H_i), cubic (C_i) and mixed/disordered (M_i) regions is found. This part corresponds quite well to the theoretical phase diagram in the left. The bottom shows the microemulsion region, which is also enlarged. The central triangle is a one-phase microemulsion, while the three surrounding regions are two-phase. This part of the phase diagram resembles the phases found in Fig. 4.*

region because entropy favors mixing for low and high concentrations.

While the pure diblock copolymer phase behavior resembles an amphiphilic system already there is a polymer system, which comes even closer to the behavior of a microemulsion. This system consists of two immiscible homopolymers (i.e. chains with only one type of segments) and a diblock copolymer with the same building blocks as the homopolymers. The first studied system is the PEO/PEP/PEO-PEP mixture (PEO is polyethyleneoxide, and PEP is polyethylene-propylene – a saturated polyisoprene). Figure 14a shows the predicted phase diagram basing on a simple theory (similar to eq. 4). There are again lamellar, hexagonal, cubic and disordered regions. The experimental phase diagram finds even two gyroid regions and a microemulsion phase. In this sense the phase diagram is highly similar to Figures 4 and 6. The phases have been identified by scattering experiments [12] by indexing the observed peaks. As for the pure diblock copolymer, the ordered phases do not show considerable coexistence regions. For very tedious experiments small coexistence regions are sometimes observed, but they are by far smaller then often predicted by theories. The highly important microemulsion phase is often dominated by fluctuations. This means that the domains are not necessarily domains of purely one segment type. The local demixing takes place only partly. Especially this character is important for applications. Very often the properties of two homopolymers shall be combined to obtain a favorable material. Most polymers are immiscible because the interactions of single segments are multiplied by the segment number, which then is larger compared to the mixing entropy. So only by quenching polymer mixtures from high to low temperatures a more or less homogenous mixture is obtained. The addition of a diblock copolymer is supporting the miscibility tremendously, which might find applications for extremely immiscible polymers. One has to keep in mind that diblock copolymers are considerably more costly than homopolymers such that industry tries to avoid them as far as possible.

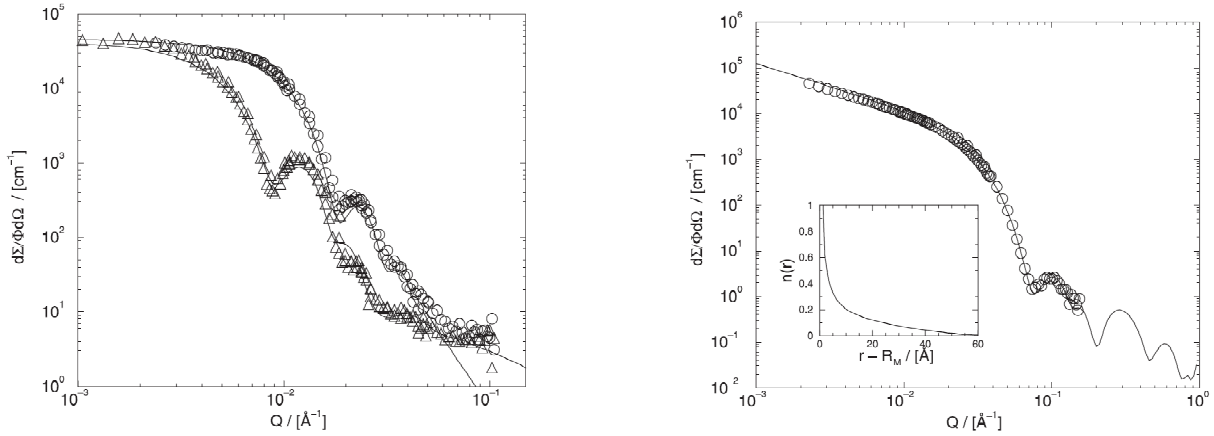

Fig. 15: *Left: Scattering of spherical polymer micelles [31] from PEP_{10}-PEO_{10} and PEP_{22}-PEO_{22}. The different curves arise from full contrast (downturn at lower/higher q for higher/lower molecular mass). Note: The forward scattering can be obtained since the curves are constant for low q. Right: Scattering of cylindrical polymer micelles from PEP_1-PEO_1. The power law q^{-1} at low q is characteristic, which indicates the 'infinitely' long domains. The inset presents the monomer density as a function of the radius.*

6 Scattering of Non-Crystalline Phases: Polymeric and Worm-Like Micelles

The scattering of ordered phases is unique and supports the identification of the different phases. For the diluted phases this high level of uniqueness is not reached, but usually the dimensions of the micelles can be extracted. So some examples will be discussed in the following.

The polymer PEP-PEO can be dissolved in water. Then the PEP forms a compact core while the PEO forms a dilute corona in the aqueous phase. As we know from simple amphiphiles there is a phase transition between spherical and cylindrical micelles. For the high molar masses spherical domains are obtained. This can be judged by the forward scattering, which is reached within our q-window. Detailed modeling of course supports the finding. For the low molar masses cylindrical domains are found. A characteristic q^{-1}-power law is found in the q-range 0.002 to 0.02Å^{-1}. This indicates relatively rigid cylindrical structures. The forward scattering is not reached in the experimental q-range, but in principle at some point the curve would reach a plateau with a finite forward scattering. So the presented experiments cannot judge about the length of the cylinders. The inset of Fig. 15b gives a radial distribution of the monomer density of the corona. In principle it is quite dilute and spans a relatively wide range to large distances. This finding supports the picture of a compact core and a dilute corona.

The best way to get access to the core and shell structure is small angle neutron scattering. The core polymer block is deuterated while the corona block is protonated. By using different compositions of H_2O and D_2O each structure can be made visible. In the full contrast (H_2O) basically the whole polymer is visible. For the core, intermediate and shell contrast, increasing amounts of D_2O were used. Results of such a study are shown in Fig. 16. In the left figure, almost spherical micelles are found because the scattering curves are nearly flat at small q. In the right figure, cylindrical micelles are found, which is indicated by the q^{-1}-power law at small scattering vectors q. The size of the compact core and the dilute corona can be directly seen from such figures. The downturn to the first minimum appears at smaller q for the core than

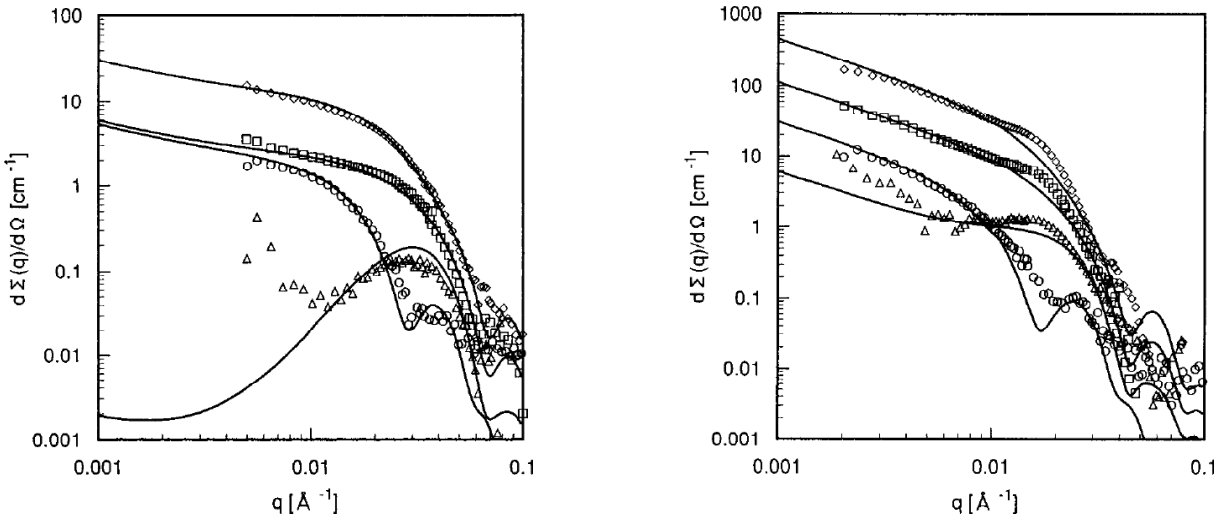

Fig. 16: *Left: Scattering of almost spherical micelles of the polymer Poly(HOVE-b-NBVE) with molar masses of 7.5 and 3 kg/mol of the core and corona forming blocks [32]. The slight inclination at small q indicates a small fraction of cylindrical micelles. The different symbols ◇, □, △, and ○ indicate the aqueous solvent being H_2O to D_2O. The corresponding contrasts are called full, core, intermediate and shell contrast. Interestingly, the intermediate contrast reaches nearly the zero-average contrast condition, which is indicated by a very low forward scattering. Right: Scattering of cylindrical micelles of the polymer Poly(HOVE-b-NBVE) with molar masses of 7.5 and 6 kg/mol of the core and corona forming blocks. The contrast conditions are the same as before.*

for the corona. Furthermore, the interesting case of nearly zero average contrast is observed. Then, the forward scattering is ideally zero, while the scattering at finite q indicates alternating structures from protonated-deuterated-protonated regions (according to the corona-core-corona structure). Macroscopically, the degree of deuteration in the whole sample is the same while locally the micelle structure appears. From the scattering contrast variation experiment and the simultaneous description of the scattering curves one obtains more precisely the different structures of the core and corona. In the simplest case one finds two radii. Especially for the corona one usually needs to assume a rather wide distribution of the segments, and so the model usually carries more information than a simple radius.

A theoretical model for polymeric micelles was formulated by Halperin [33]. It bases on three contributions to the free energy. The first contribution considers the corona. Close to the core the polymers are anchored densely enough such that a polymer gel is formed. This gel has a typical mesh size, which increases to the outer regions. Each polymer part inside such a mesh is called a blob and contributes with 1 k_BT to the free energy. The second contribution comes from the polymer stretching inside the core. Here, the equilibrium chain dimension of a melt has to be compared with the polymer size in the real core. The polymer is seen as an entropic spring. The relative size gives rise to an entropic contribution to the free energy. The last contribution is the surface tension of the core with respect to the aqueous region. Here, simply the core surface times a classical surface tension yields the enthalpic contribution to the free energy. From such a model the free energy is minimized to yield the aggregation number N_{agg}, from which all dimensions and the shape of the micelle can be determined.

So far we have only described rigid cylindrical micelles. Locally, very often the micelles stay

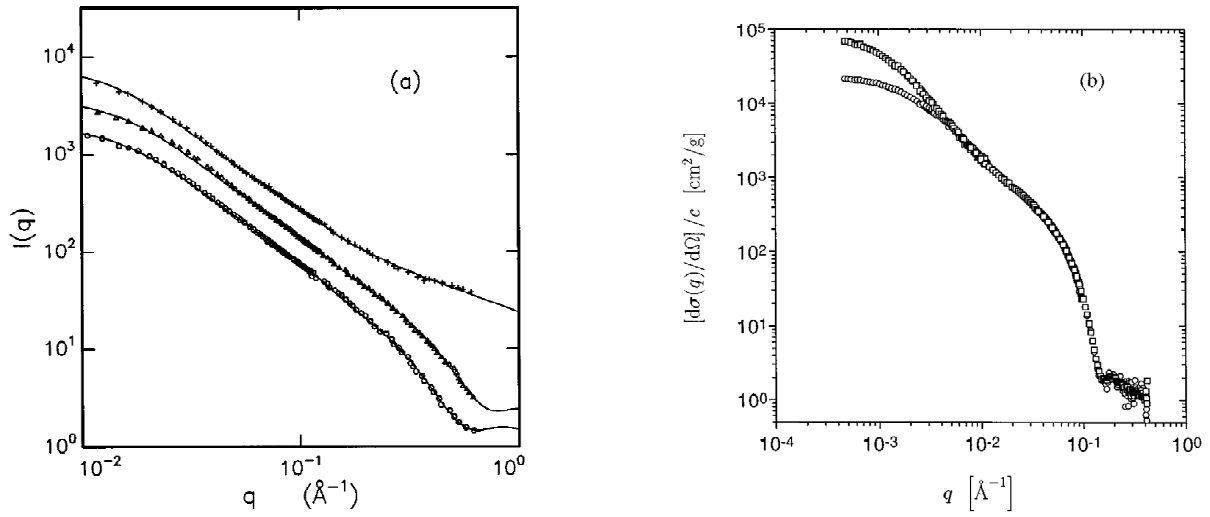

Fig. 17: *Left: The polymer polystyrene in the good solvent CS_2 [34]. The three curves are obtained for deuterated backbone (+), deuterated phenyl ring (△), and fully deuterated chain (○). The polymer is a worm-like object and resembles worm-like micelles with a small cross section. At low $q < 0.02Å^{-1}$ the Guinier scattering observes the whole polymer. At intermediate q up to 0.2Å^{-1} the wormlike power law with $q^{-1.67}$ is observed. At high q the finite diameter of the polymer becomes visible. Right: The system water/d-isooctane/lecithin with a molar water-to-lecithin ratio of 2.5 and lecithin concentrations of 0.9 mg/ml (○) and 3.5 mg/ml (□) [4]. Wormlike micelles are formed. At low $q < 0.001Å^{-1}$ the Guinier scattering observes the whole micelle. At intermediate q up to 0.02Å^{-1} the wormlike power law with $q^{-1.67}$ is observed. At slightly higher q up to 0.05Å^{-1} the local rigidity is indicated by a q^{-1}. At high q the finite diameter of the micelle is observed.*

rigid while on larger length scales the fluctuations lead to the loss of correlations. In the extreme case, then the micelle follows a random walk. This concept is also known from polymers (and diffusion processes). A polymer in a solvent with zero exchange interaction (theta solvent) shows the fractal structure of the polymer with a q^{-2} dependence. Here the self-similarity of sub-sections with the whole polymer is expressed. The exponent -2 arises from the following: A random walk lacks correlations between individual steps. For the ensemble averaged squared end-to-end distance R^2_{ee} one obtains the proportionality to the number of steps N (see also Chapter B1). Thus, the segment number as a function of the length scale carries the exponent 2. The scattering intensity is proportional to the number of scatterers while the length scale is connected with the reciprocal q vector. Fig. 17a shows the example of a polymer in a good solvent. Accordingly, the power law changes from q^{-2} to $q^{-1.67}$ for the Flory chain. The excluded volume interactions are responsible for this power law, which means the intersections of the chain appear in the free energy as an important contribution. The other example of Fig. 17b shows the scattering experiment from an inverse micelle formed by water/d-isooctane/lecithin. Again, a clear power-law for the worm-like micelle with excluded volume interactions is observed. Apart from that, a small q-range at slightly higher q indicates the still locally rigid micelle. Both examples are very good, because the whole object is observed in the Guinier range at lowest q. From the forward scattering $I(q \to 0)$ the connection to the concentration ϕ and the volume of the particle (i.e. polymer or micelle) can be made. In the simplest case one finds $I(q \to 0) \propto \phi V_{\mathrm{particle}}$. In reference [4] a more complicated renormalization theory is

applied. The other parameter of the Guinier-range is the overall size of the worm-like object, i.e. $R_{\mathrm{ee}} = \sqrt{6} \cdot R_{\mathrm{g}}$. Scattering scientists usually prefer the radius of gyration R_{g} instead of the end-to-end distance. Furthermore, at high q the small scale structure of the polymer or the micelle is indicated. For the micelle it is a simple circular cross-section. For the polymer a more atomistic model has to be taken into account. The overall example of worm-like objects shows that many structural parameters can be obtained from a single scattering experiment. The power laws give clear hints to the kind of structure formed. A good model is highly recommended to extract the structural parameters to the highest precision possible.

7 Polymer Boosting Effect

The polymer boosting effect was first observed by phase diagram measurements [35]. For characterizing the efficiency of a surfactant equal amounts of water and oil are mixed with a variable amount of surfactant ϕ_{C}. Then the phases are determined as a function of temperature for each ϕ_{C}. Such a phase diagram is displayed in Fig. 18. Without polymer there is a one-phase region (fish-tail) with a minimum amount of surfactant, which is needed to solubilize the water and oil. This surfactant amount is a characteristic figure for the efficiency of a surfactant. When adding polymer as a fourth component the total amphiphile concentration $\phi_{\mathrm{C+D}}$ is the considered variable. The relative amount of the polymer is given in units $\delta = m_{\mathrm{polymer}}/(m_{\mathrm{surf}} + m_{\mathrm{polymer}})$, which takes values of 1.4 to 10%. However, the absolute values in the overall microemulsion are tiny and take values from 0.2 to 0.4%. Nonetheless, these small amounts of polymer are responsible for the one-phase region to move to smaller amphiphile concentrations. This means the diblock copolymer makes the surfactant more efficient. Using small angle neutron scattering experiments under contrast variation [37] it could be proved that the diblock copolymer is anchored in the surfactant membrane. So each block finds the way in the domain where it is soluble, and takes a mushroom-like conformation. Due to its anchoring the polymer exerts a pressure on the membrane, which is responsible for an effectively higher membrane rigidity. This leads to the formation of larger domains with a better surface to volume ratio. This is the quick explanation for the polymer boosting effect, which we shall discuss in more details now. We have already seen that the free energy of a microemulsion is dominated by the elastic behavior of the membrane [**?**]. There are two moduli κ and $\bar{\kappa}$, which describe the energy needed to deform the membrane with a certain mean curvature and a saddle splay curvature. For simplicity, we assume that the equilibrium curvature c_0 is zero, which is true for the phase inversion temperature, the temperature of the fish-tail-point. The bending rigidity depends on different physical contributions as we will see now [38]:

$$\begin{aligned} \frac{\kappa_R}{k_B T} &= \frac{\kappa_0}{k_B T} && \text{pure membrane} \\ &+ \frac{\alpha}{4\pi} \ln(\psi) && \text{thermal fluctuations} \\ &- 0.0238 \frac{\phi_p (R_{hW}^3 + R_{hO}^3)}{V_p} && \text{homopolymer} \\ &+ \frac{1}{12} \left(1 + \frac{\pi}{2}\right) \sigma (R_{dW}^2 + R_{dO}^2) && \text{diblock copolymer} \end{aligned} \tag{7}$$

The first contribution arises from the membrane itself. The surfactant molecules withstand deformations due to their molecular structure. The next addend describes the spatial renormalization. Due to the fluctuations of the membrane the membrane looks less rigid on larger length

scales ($\alpha = 3$). The negative sign arises from the logarithm of the membrane volume fraction $\psi = \phi_C - 0.01 < 1$, which is the total surfactant content minus the unimerically dissolved surfactant. While corrugated paper looks more stiff on larger length scales the membrane shows the opposite effect. The next contribution describes the homopolymer effect. It is proportional to the homopolymer concentration ϕ_p, the cubed end-to-end distances of the water and oil soluble polymers R_{hW} and R_{hO} and the reciprocal volume of the polymer V_p. The last addend is the diblock copolymer contribution. It is proportional to the grafting density σ (no. of polymers per membrane area) and the squared end-to-end distances of the water and oil soluble blocks R_{dW} and R_{dO}. The theoretical effect is also depicted in Fig. 19 where diblock copolymers exert a pressure on the membrane, which leads to flattening. Contrarily, homopolymers facilitate the fluctuations of the membrane. The saddle splay modulus in principle has the same dependency as κ, according to:

$$\frac{\bar{\kappa}_R}{k_B T} = \frac{\bar{\kappa}_0}{k_B T} + \frac{\bar{\alpha}}{4\pi} \ln(\psi) + 0.0211 \frac{\phi_p (R_{hW}^3 + R_{hO}^3)}{V_p} - \frac{1}{6} \sigma (R_{dW}^2 + R_{dO}^2) \tag{8}$$

It should be emphasized that the three contributions from fluctuations ($\bar{\alpha} = -10/3$), and the polymers are very similar in magnitude but they have opposite signs as for κ. So one can roughly say that κ and $\bar{\kappa}$ have the same value but opposite signs. The moduli now have to be connected to observable effects in order to compare them. From molecular dynamics simulations the saddle splay modulus takes a certain value at the fish tail point, i.e. $\bar{\kappa}_R = \bar{\kappa}_{\mathrm{FTP}}$. This value is much smaller than the intrinsic surfactant molecule contribution $\bar{\kappa}_0$, and so $\bar{\kappa}_{\mathrm{FTP}}$ can be neglected. So equation 8 can be solved for the surfactant content, which will read then:

$$\psi = \psi_0 \exp\left(\bar{\beta} \frac{\phi_p}{V_p} (R_{hW}^3 + R_{hO}^3) - \bar{\Xi} \sigma (R_{dW}^2 + R_{dO}^2) \right) \tag{9}$$

The minimum surfactant concentration of the pure system arises from the constant $\bar{\kappa}_0$, and can be measured directly. The coefficients $\bar{\beta}$ and $\bar{\Xi}$ are derived from equation 8 by dividing by $\bar{\alpha}$. It is directly obvious that adding diblock copolymer leads to smaller amounts of surfactant needed to solubilize oil and water while homopolymers show the opposite effect. Thus, starting from the Helfrich free energy we have explained how the polymer boosting effect works. But we are still left with the connection of κ to experiments. If one conducts small angle neutron scattering experiment on bicontinuous microemulsions one observes typical scattering curves as depicted in Fig. 20. There is a pronounced peak at a scattering vector q^*, which is connected with the domain spacing $d \approx 2\pi/q^*$. The width of the peak is proportional to the reciprocal correlation length ξ. At small angles there is still considerable forward scattering. So, the microemulsion does not only have alternating domains with a periodicity d, but also long range fluctuations. This arises from local enrichments of water or oil because the surfactant does not fully make sure that the local concentration is the overall concentration. The forward scattering is also directly proportional to the reciprocal osmotic compressibility. At large q there is the Porod law $I(q) \propto Pq^{-4}$, which comes from the sharp surfaces of the water and oil domains. The Porod constant P is proportional to the surface per volume $S_{\mathrm{tot}}/V_{\mathrm{tot}}$, and, therefore, is proportional to the membrane volume content ψ. The overall scattering function is well described by the following formula:

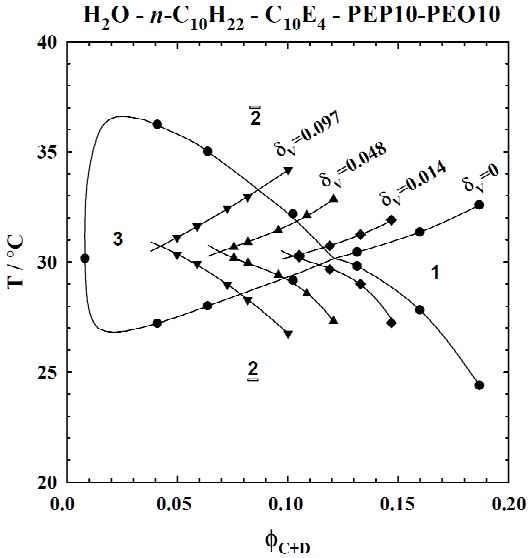

Fig. 18: *Phase diagram: Temperature as a function of the amphiphile content $\phi_{\mathrm{C+D}}$. The phase diagram without polymer (●) shows different regions: At high and low temperatures there are two-phase coexistence regions ($\bar{2}$ and $\underline{2}$). For intermediate temperatures at higher surfactant contents there is the one-phase bicontinuous microemulsion (1). For intermediate temperatures at low surfactant contents there is the three-phase coexistence region (3) with a microemulsion coexisting with a water-rich and an oil-rich phase. Furthermore, there are the one-phase boundaries (fish-tails) shown for additions of amphiphilic diblock copolymer at concentrations of $\delta = 0.014(\blacklozenge), 0.048(\blacktriangle)$ and $0.097(\blacktriangledown)$. The added polymer was PEP_{10}-PEO_{10}.*

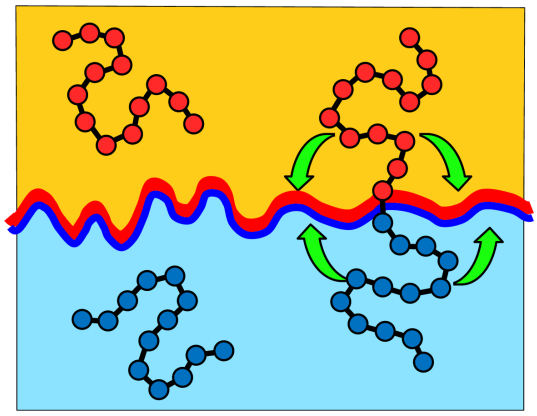

Fig. 19: *Scheme of homopolymers and diblock copolymers at a surfactant membrane in a microemulsion. The homopolymer favors membrane fluctuations while the diblock copolymer exerts a pressure on the membrane, which causes flattening.*

$$I(q) = \frac{d\Sigma}{d\Omega}(q) = \left(\frac{8\pi\langle\nu^2\rangle/\xi}{q^4 - 2(k_0^2 - \xi^{-2})q^2 + (k_0^2 + \xi^{-2})^2} + \frac{G \cdot \mathrm{erf}^{12}(1.06qR_g/\sqrt{6})}{1.5q^4R_g^4} \right) \exp(-\sigma^2q^2) + b_{\mathrm{backgr}} \quad (10)$$

The normalized intensity $I(q)$ is given by the macroscopic scattering cross section $d\Sigma/d\Omega$. The first fraction in the top line of equation 10 describes the long wavelength behavior for wavelengths down two approximately q^*, i.e. the domain spacing. This expression is known as the Teubner-Strey theory [39]. The term arises from a Landau description of the order parameter, similar to eq. 4. The Landau approach assumes that the free energy can be described as a

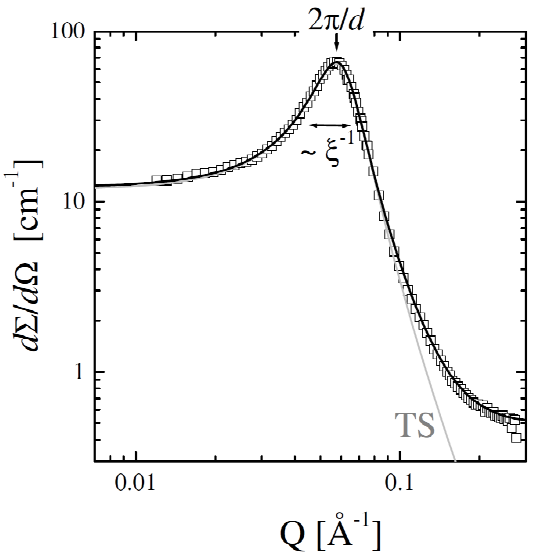

Fig. 20: *A typical scattering pattern of a bicontinuous microemulsion (intensity vs. q) in bulk contrast, i.e. with D_2O, hydrogenated oil and hydrogenated surfactant [40]. From the peak position the domain spacing is derived, while the peak width indicates the correlation length. The grey curve shows the fit with the Teubner-Strey theory. The solid line is a fit with the extended theory of equation 10.*

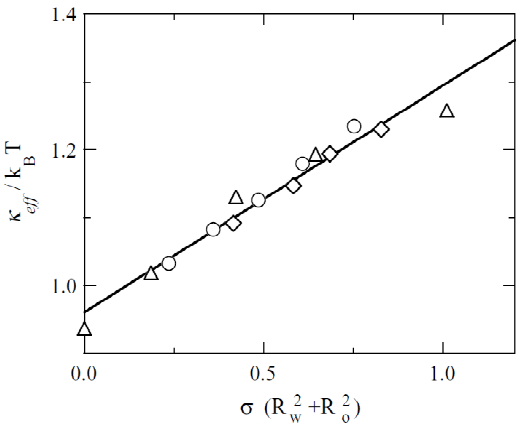

Fig. 21: *The bending rigidity κ as a function of the scaled diblock copolymer amount [36]. According to equation 7 this function is linear. It shows that the membrane becomes more rigid with the diblock copolymer addition. Different symbols arise from different molar masses of the polymer.*

functional expansion of the order parameter(s). From symmetry considerations, and considerations about the highest order terms needed, one usually arrives at rather simple expressions. Using the Fluctuation-Dissipation Theorem the scattering function can be calculated from the free energy. This basically leads to the fourth order polynomial in the denominator. From the real space correlation function it then can be judged, which structural information is found in the coefficients [37]. Here the real wave number $k_0 = 2\pi/d$ appears, which is only approximately the peak position q^*. The corellation length ξ is also well defined now. The numerator is connected to the scattering length density difference $\Delta\rho$ and the water-water correlation average, according to $\langle\nu^2\rangle = (\Delta\rho)^2\phi_W(1-\phi_W)$ with ϕ_W being the water content. The second fraction in equation 10 describes additional surface [40], which is not expressed by the Landau approach, which is obvious because the approach comes from long wavelengths and does not cover the exact domain structure. So the sharp transition from water $(+1)$ to oil (-1) is not well described, and the short wavelength fluctuations shorter than the domain spacing are not well covered either. The expression is rather phenomenological, but was motivated in another context with fractal structures by Beaucage. His approach described the long wavelength behavior by a Guinier approach, and the short wavelength behavior was exactly this term we find here, except that we restricted ourselves to the Porod behavior for sharp surfaces. Here, the radius of gyration R_g describes the size of a single domain (i.e. $R_g \sim d/2$). The amplitude G is correlated with the amount of additional surface while the overall Porod constant is given by $P = 8\pi\langle\nu^2\rangle/\xi + G/(1.5R_g^4)$. The error function $\mathrm{erf}(x)$ is connected to the integral of a Gauss peak. In case that the surfactant molecules are slightly excited individually, the exponential fac-

tor takes care of this. Usually, this kind of roughness is described by a length of $\sigma = 2$Å, which is practically invisible for most of the examples. The last addend describes the incoherent background. Mostly, the scattering curves are measured for large enough q, such that the constant level b_{backgr} is well defined. From the scattering experiment we obtain the structural parameters k_0 and ξ. The Gaussian Random Fields Theory [37] connects the structural parameters with the bending rigidity according to:

$$\frac{\kappa_R}{k_B T} = \frac{5\sqrt{3}}{64} k_0 \xi \tag{11}$$

Within the derivation the assumption was made that the bending rigidity is large enough, otherwise a more complicated function will appear. From practical applications formula 11 appeared quite precise [37]. Now, the obtained bending rigidity κ can be compared with the model (see Fig. 21). We obtain a linear increase as a function of the scaled polymer amount. This means that diblock copolymers stiffen the membrane. From literature [37] it is known that the logarithm of the minimum surfactant amount shows the same linear behavior according to eq. 9. This shows that two different observations (scattering and phase diagram) can be compared on the same level through the microscopic interpretation via the Helfrich free energy.
While diblock copolymers are quite expensive for industrial applications a simpler way for synthesizing amphiphilic polymers was found. Starting from a linear long alcohol (like dodecanol) the water soluble block can be polymerized quite easily. This yields an amphiphilic polymer with a short hydrophobic part (C_{12}) and a polymer-like water soluble part. This kind of polymer is cheap to produce and it is highly water soluble. The latter is important for formulations because the symmetric diblock copolymer dissolves only very slowly. The slight unsymmetry results in a small equilibrium curvature, which is compensated by slightly higher temperatures. So, even for applications a suitable polymer was found.

8 Microemulsions Near Planar Walls

Surfaces are highly important for the application of microemulsions. This is obvious for cleaning processes because the fluid shall take up the dirt from the surface. But also in enhanced oil recovery applications there are huge surfaces from the sand stone where the oil is located. For instance the cracking fluid is an aqueous surfactant system with wormlike micelles. The micelle network leads to a high viscosity. With this high viscosity the pressure energy can be deposited in the sand stone, which leads to crack formation. To the cracks sand particles (the proppant) are transported to avoid the collapse of the cracks after the application. The aqueous surfactant solution forms a microemulsion in contact with oil, which has a low viscosity. After the application oil can be produced at a higher speed.
So, one important model system to study is a bicontinuous microemulsion adjacent to a hydrophilic planar wall [41]. This question was addressed by computer simulations [41]. A real space picture is shown in Fig. 22. One can see the lamellar order near the surface and the bicontinuous microemulsion in the volume. A kind of order parameter is obtained by laterally averaging the structure as a function of the depth (Fig. 23). Here, two perfect lamellae are observed before the order decays into the volume where an average is reached. This decay is what one would expect for a lamellar order induced by a surface. The real question is how the decaying order of the lamellae is realized. From the lateral cuts in the bottom of Fig. 23 we see that there are perforations in the lamellae, which lead to the decreasing order. At this point, the

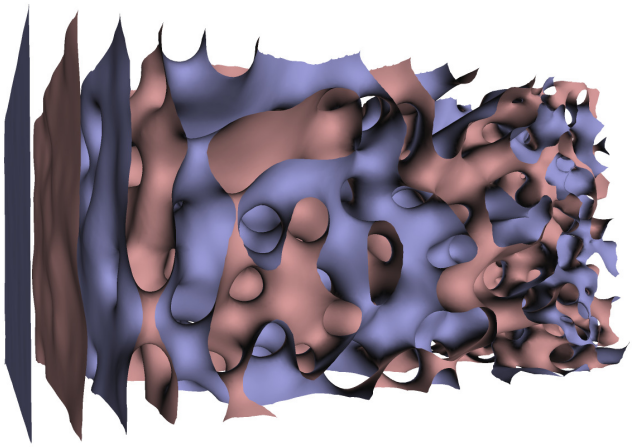

Fig. 22: *A real space image of a microemulsion near a planar hydrophilic wall from a computer simulation [41]. The surfactant layer is depicted with blue and red facing the water and oil domains. Close to the surface a lamellar order is formed while in the volume the microemulsion is bicontinuous.*

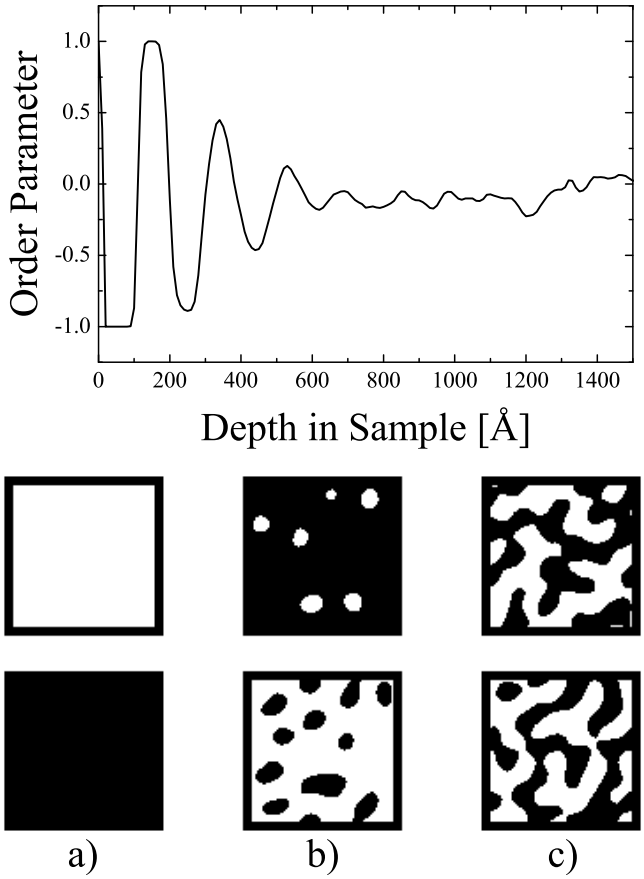

Fig. 23: *Top: The laterally averaged structure of the microemulsion near a planar wall. This function looks like an order parameter of a decaying lamellar order. Bottom: Lateral cuts in different depths (< 100, ~ 300, and 1000Å). There is a) perfect lamellar order, b) perforated lamellae, and c) bicontinuous microemulsion.*

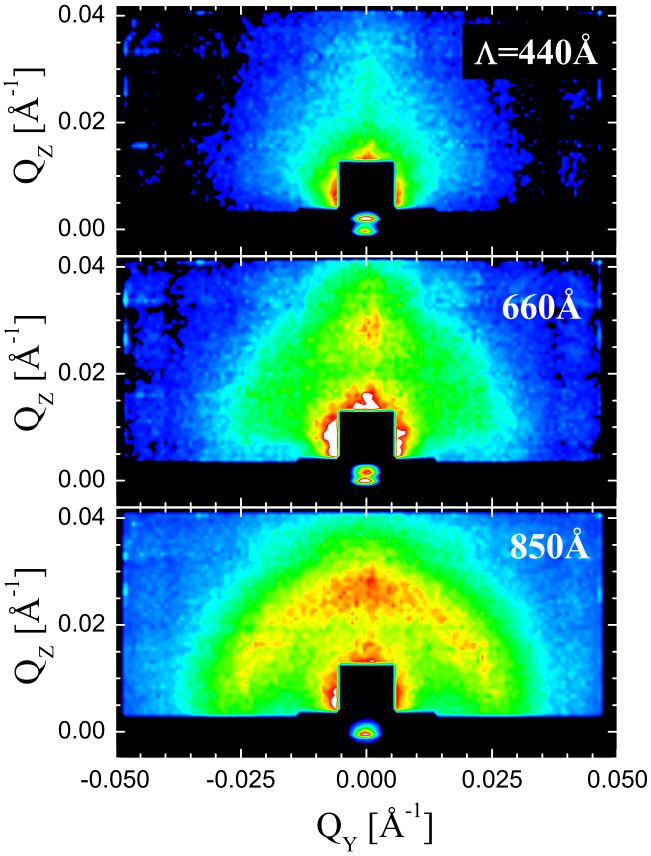

Fig. 24: *GISANS patterns at different penetration depths* Λ. *For 440Å there is a rather strong surface scattering background in the center and a lamellar peak is only slightly indicated in the middle top. For 660Å the lamellar peak becomes stronger. For 850Å both the lamellar peak and the bicontinuous Debye-Scherrer ring are visible.*

perforated lamellae of a diblock copolymer shall be recalled (Fig. 13). Nonetheless, we believe that the perforations in the microemulsion are a transition state, which is not stable.

A microemulsion was studied by grazing incidence small angle neutron scattering (GISANS) and reflectometry experimentally. The reflectometry measurements basically confirm the decaying order parameter of the simulations. The GISANS experiments are also sensitive to the lateral structures and so there were contributions from the bicontinuous region as well (Fig. 24). Small angle scattering with grazing incidence leads to an evanescent (tunneling) wave in the sample. So the sample is illuminated with a variable depth. This depth depends on the scattering length density difference of the silicon block, which provides the solid-liquid surface and the overall microemulsion. Furthermore, the incident angle allows for fine-tuning the penetration depth of the evanescent wave. In the current study the penetration depth Λ was varied between ca. 400 and 1000Å. For small Λ the surface scattering dominates the signal, and the lamellar structure appears only weakly with a Bragg peak. At intermediate $\Lambda \approx 660$Å the Bragg peak becomes more prominent. At higher Λ the bicontinuous microemulsion becomes visible as well. From this experiment the integral intensities of the Bragg peak and the Debye-Scherrer ring are determined. Their ratio is plotted in Fig. 25. The experimental points show an increasing linear behavior from penetration depths of 400Å on where the bicontinuous phase starts to be visible. So the well ordered lamellar phase covers the first 400Å. For the computer

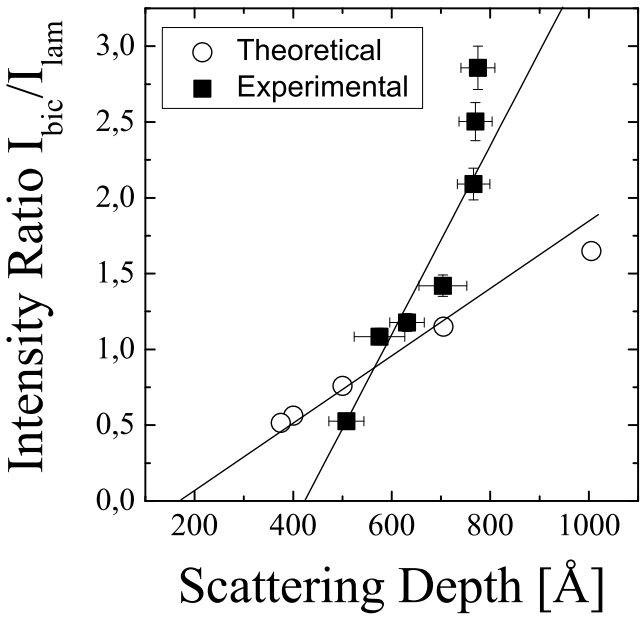

Fig. 25: *The integral intensity ratio of the bicontinuous and the lamellar structure as obtained from GISANS experiments (■). At a penetration depth (scattering depth) Λ of ca. 400Å the ratio starts to grow linearly. This value indicates the beginning of the perforated lamellae. For the simulations (○) the ratio starts to grow already at 200Å where the perforated lamellae are found explicitely.*

simulations the same plot shows that the characteristic depth is ca. 200Å. From the real space structure it is known that from this depth on the perforated lamellae expand. The reason is that the typical length scale of the perforations is nearly the same as for the bicontinuous structure (see Fig. 23). So the GISANS experiment determines the beginning of the perforated lamellae because it appears like an isotropic structure.

9 Pickering Emulsions and Ianus Particles

So far we have seen surfactant molecules and diblock copolymers forming self-assembled structures on the nano scale. Basis for this effect was the amphiphilicity, which favored the formation of hydrophilic and hydrophobic domains, which show a stronger or weaker kind of organization. This concept does not only hold on the nano scale. Certain particles in the sub-micrometer scale can form self-assembled structures on the micrometer scale. The simplest particle is a homogenous sphere. If the surface tensions of water/particle and oil/particle are chosen right the particles tend to cover the surface of the oil and water domains and, thus, pickering emulsions [42] are obtained (Fig. 26). So even non-amphiphilic meso-particles can stabilize emulsions. Their advantage is that the particles leave space for exchanging substances between the hydrophilic and hydrophobic volumes. The pickering emulsions might be used if the final product of a process must not have impurities from surfactants.
The pickering emulsions can also be used as templates to produce amphiphilic meso-particles, the Ianus particles [42]. A good review about Ianus particles is given in Reference [43]. Ianus was a god with two faces for the ancient Romans. The two faces stand for the amphiphilic-

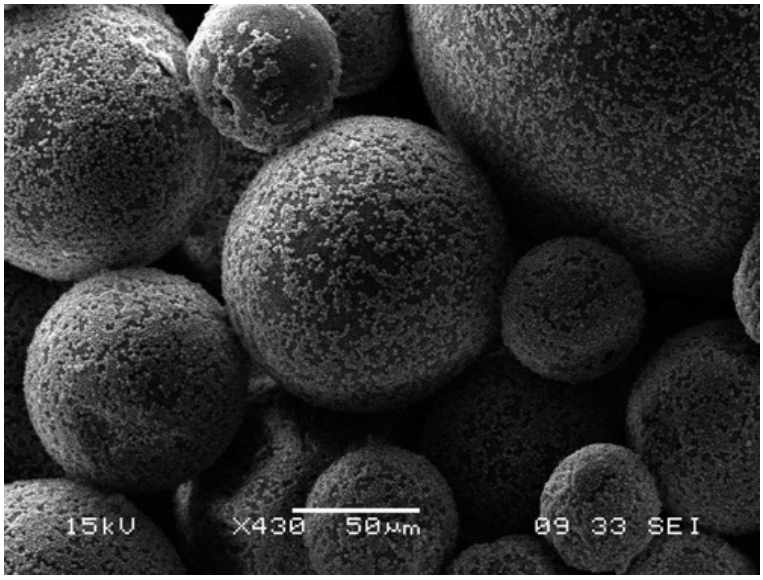

Fig. 26: *A transmission electron micrograph of a pickering emulsion [42]. Spherical wax domains are surrounded by the untreated silica particles and dispersed in water.*

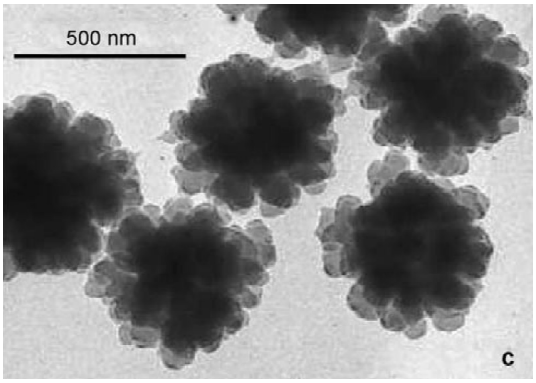

Fig. 27: *Transmission electron micrograph of a micelle formed by Janus particles [44]. Especially the outer water soluble regions of the particles become clearly visible.*

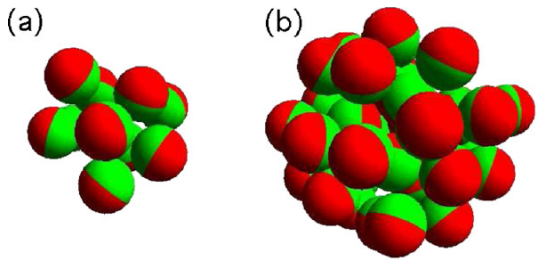

Fig. 28: *Structure of micelles formed by Janus particles from computer simulations [45]. There exist (a) spherical micelles and (b) vesicles similar as for surfactant molecules.*

ity of the meso-particles. These particles now have very similar properties as surfactants or amphiphilic molecules. So, they stabilize emulsions by forming a layer around the domains. Again, these emulsions leave some space for exchange of substances between both domains. But also the pure particles in aqueous solution form micelles [44] alike surfactants (Fig. 27). These micelles have also been investigated theoretically [45]. Besides simple micelles also vesicles are predicted (Fig. 28).

The variety of practically produced Janus particles is large. Very often amphiphilic polymers play a role, or the particles are synthesized from (micro)emulsions. The particles may have several patches – not only two. Then strings and networks of the meso-particles are obtained. So the options for Janus particles are maybe even larger than for simple surfactants. Due to the high effort of the synthesis not many applications are known.

10 Summary

We have seen that there exist single molecules with chemical groups, which dislike each other. This property is called amphiphilicity. Surfactants are the most widely used substance with hydrophilic heads and hydrophobic tails. There exist ionic and non-ionic surfactants. Surfactants need to cross the critical micelle concentration to form micelles with various shapes. These shapes already have a high degree of symmetry because the surfactant molecules are all identical. At high concentrations interactions between the micelles come into play and liquid crystalline ordering takes place. These structures have again a high degree of symmetry, again because of identical building blocks.

Microemulsions involve two kinds of solvents and enlarge the variety of phases (or shapes) found in the phase diagram. Domains of water and oil form with a surfactant layer in between. The theoretical concept of Helfrich treats the surfactant layer as an elastic membrane with negligible thickness. Very important are bicontinuous phases where domains expand over macroscopic distances.

Polymers can also be treated with the concept of amphiphilicity even when the interactions are much weaker. The large number of segments leads to effectively strong enough interactions in comparison to the entropy of mixing. Interestingly, polymeric microemulsions exist as well. Micelles of amphiphilic polymers can be obtained when dissolving in water. The water soluble parts form a hairy corona.

Amphiphilic block copolymers as additives in a microemulsion lead to the polymer boosting effect. The efficiency of the surfactant is dramatically increased. The diblock copolymer exerts a pressure on the surfactant membrane, which leads to flattening. Thus, larger domains can be formed with a better surface to volume ratio.

Microemulsions tend to form a lamellar order near planar walls. The decay of the lamellar order is realized by perforations in the lamellae.

Meso-particles can also be used to obtain self-assembly. The pickering emulsions are formed with homogenous particles. The particle layer on the domain surface allows for the exchange of substances. The Ianus particles have a similar behavior as surfactant molecules.

Scattering experiments support the structure identification. They give length parameters in a direct way while averaging over a large sample volume. The connection to microscopic theories reveals the mechanisms of amphiphilic molecules. This understanding is supporting the next generation of applications when simple formulation experiments do not succeed anymore.

Polymers are the key additives to amphiphilic systems of the future. While in this manuscript only linear amphiphilic polymers were introduced the diversity of possible architectures is huge. Specific architectures allow to tailor polymers for very specific applications. At the moment we are only at the beginning of a promising story of basic research.

References

[1] J.S. Keiper, R. Simhan, J.M. DeSimone, G.D. Wignall, Y.B. Melnichenko, H. Frielinghaus, *J. Am. Chem. Soc.* **124**, 1834 (2002)

[2] A.-G. Fournial, Y. Zhu, V. Molinier, G. Vermeersch, J.M. Aubry, N. Azarouali, *Langmuir* **23**, 11443 (2007)

[3] J.N. Israelachvili, D.J. Mitchell, B.W. Ninham, *J. Chem. Soc. Faraday Trans. I* **72**, 1525 (1976)

[4] J.S. Pedersen, S.U. Egelhaaf, P. Schurtenberger, *J. Phys. Chem.* **99**, 1299 (1995) and G. Jerke, J.S. Pedersen, S.U. Egelhaaf, P. Schurtenberger, *Phys. Rev. E* **56**, 5772 (1997)

[5] R. Strey, R. Schomäcker, D. Roux, F. Nallet, U. Olsson, *J. Chem. Soc. Faraday Trans.* **86**, 2253 (1990)

[6] E. Jahns, H. Finkelmann, *Colloid & Polymer Sci.* **265**, 304 (1987)

[7] R. Strey, *Phys. Chem. Chem. Phys.* **97**, 742 (1993)

[8] H.T. Davis, J.F. Bodet, L.E. Scriven, W.G. Miller, *Physica A* **157**, 470 (1989)

[9] Internal communication with M. Kraus, G. Goos, and G. Gompper; see also G. Gompper, M. Kraus, *Phys. Rev. E* **47**, 4301 (1993) and G. Gompper, G. Goos, *Phys. Rev. E* **50**, 1325 (1994)

[10] R.G. Larson, *J. Chem. Phys.* **91**, 2479 (1989)

[11] G.J.T. Tiddy, *Physics Reports* **57**, 1 (1980)

[12] N.R. Washburn, T.P. Lodge, F.S. Bates, *J. Phys. Chem. B* **104**, 6987 (2000)

[13] W. Helfrich, *Z. Naturforsch., A: Phys. Sci.* **33**, 305 (1978)

[14] S.A. Safran, L.A. Turkevich, P. Pincus, *J. Physique, Lettres* **45**, L-69 (1984)

[15] E.M. Blokhuis, W.F.C. Sager, *J. Chem. Phys.* **115**, 1073 (2001)

[16] U.S. Schwarz, G. Gompper, *Phys. Rev. E* **59**, 5528 (1999)

[17] U.S. Schwarz, G. Gompper, *Phys. Rev. Lett.* **85**, 1472 (2000)

[18] R.R. Netz, D. Andelman, M. Schick, *Phys. Rev. Lett.* **79**, 1058 (1997)

[19] F. Schwabl, *Statistical Mechanics* (Springer, Berlin, Heidelberg, New York, 2002)

[20] W.B. Lee, R. Mezzenga, G.H. Fredrickson, *Phys. Rev. Lett.* **99**, 187801 (2007)

[21] X.J. Li, M. Schick, *Biophys. J.* **78**, 34 (2000)

[22] C. Stubenrauch, C. Frank, R. Strey, D. Burgemeister, C. Schmidt, *Langmuir* **18**, 5027 (2002)

[23] T. Hahn, Ed. *International Tables for Crystallography, 5th ed.* (Kulver, Dordrecht, The Netherlands, 2002)

[24] S. Förster, A.K. Khandapur, J. Zhao, F.S. Bates, I.W. Hamley, A.J. Ryan, W. Bras *Macromolecules* **27**, 6922 (1994)

[25] S. Abbas, T.P. Lodge, *Langmuir* **24**, 6247 (2008)

[26] K.D. Göcking, M. Monkenbusch, *Europhys. Lett.* **43**, 135 (1998)

[27] F. Castro-Roman, L. Porcar, G. Porte, C. Ligoure, *Eur. Phys. J. E* **18**, 259 (2005)

[28] R. Hosemann, S.N. Bagchi, *Direct Analysis of Diffraction by Matter* (North-Holland, Amsterdam, 1962)

[29] Y.Y. Huang, J.Y. Hsu, H.L. Chen, T. Hashimoto, *Macromolecules* **40**, 406 (2007)

[30] A.K. Khandpur, S. Förster, F.S. Bates, I.W. Hamley, A.J. Ryan, W. Bras, K. Almdal, K. Mortensen, *Macromolecules* **28**, 8796 (1995)

[31] H. Kaya, L. Willner, J. Allgaier, J. Stellbrink, D. Richter, *Appl. Phys. A* **74**, S499 (2002)

[32] M. Nakano, H. Matsuoka, H. Yamaoka, A. Poppe, D. Richter, *Macromolecules* **32**, 697 (1999)

[33] A. Halperin, *Macromolecules* **20**, 2943 (1987)

[34] J.S. Pedersen, P. Schurtenberger, *Macromolecules* **29**, 7602 (1996)

[35] B. Jakobs, T. Sottmann, R. Strey, J. Allgaier, L. Willner, D. Richter, *Langmuir* **15**, 6707 (1999)

[36] H. Endo, J. Allgaier, G. Gompper, B. Jakobs, M. Monkenbusch, D. Richter, T. Sottmann, R. Strey, *Phys. Rev. Lett.* **85**, 102 (2000)

[37] H. Endo, M. Mihailescu, M. Monkenbusch, J. Allgaier, G. Gompper, D. Richter, B. Jakobs, T. Sottmann, R. Strey, I. Grillo, *J. Chem. Phys.* **115**, 580 (2001)

[38] D. Byelov, H. Frielinghaus, O. Holderer, J. Allgaier, D. Richter, *Langmuir* **20**, 10433 (2004)

[39] M. Teubner, R. Strey, *J. Chem. Phys.* **87**, 3195 (1987)

[40] C. Frank, H. Frielinghaus, J. Allgaier, H. Prast, *Langmuir* **23**, 6526 (2007)

[41] M. Kerscher, P. Busch, S. Mattauch, H. Frielinghaus, D. Richter, M. Belushkin, G. Gompper, *Phys. Rev. E*, accepted for 2011

[42] L. Hong, S. Jiang, S. Granick, *Langmuir* **22**, 9495 (2006)

[43] F. Wurm, A.F.M. Kilbinger, *Angew. Chem. Int. Ed.* **48**, 8412 (2009)

[44] L. Nie, S. Liu, W. Shen, D. Chen, M. Jiang *Angew. Chem. Int. Ed.* **46**, 6321 (2007)

[45] F. Sciortino, A. Giacometti, G. Pastore, *Phys. Rev. Lett.* **103**, 237801 (2009)